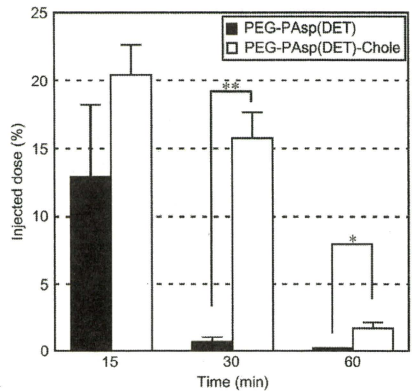


**Fig. 10.** (A) Relative diffusion time of PEG-PAsp(DET)-Alexa680-Chole block copolymers and their polyplex micelles in the Hepes buffer (pH 7.3). Closed bars: 18.7 μg/mL of block copolymers in the solution. Open bars: 2.08 μg/mL of block copolymers in the solution. (B) Percentage of PEG-PAsp(DET)-Alexa680-Chole block copolymers associating with pDNA in the micelle solutions at different pH. Closed bars: Hepes buffer (pH 7.3). Open bars: MES buffer (pH 5.5). Polyplex micelles were prepared at N/P = 8. Error bars in the graph represent SEM, n = 7. \**P* < 0.01.

corroborates well with the result that PEG-PAsp(DET)-Chole micelles achieved high gene transfer under the diluted conditions (Fig. 7B). The amount of polymer associated with pDNA in PEG-PAsp(DET)-Chole micelles (N/P = 8) at pH 7.3 estimated by FCS (42% in Fig. 10B) was in accordance with that calculated from ultracentrifugation analysis (45% in Fig. 4), where 340 of total 756 block copolymers per pDNA were associated with a pDNA. Furthermore, the percentage of polymers associating with pDNA significantly decreased upon lowering the pH from 7.3 to 5.5 (Fig. 10B). Note that ethanediamine units in the side chain of PAsp (DET) adopt a mono-protonated form at pH 7.4 and then become di-protonated at pH 5.5 [11,12]. Thus, this change in the charge state of PAsp(DET) might lead to electrostatic repulsion among block copolymers in the polyplex micelle, thereby releasing a considerable amount of polymers associating with pDNA at pH corresponding to endosomal compartments.

**3.12. Stability of polyplex micelles in the blood stream**

In order to evaluate the stability of polyplex micelles in the blood, the concentration of Cy5-pDNA in the plasma was measured at various times after intravenous injection of polyplex micelles (N/P = 8) containing Cy5-pDNA via the tail vein of mice (Fig. 11). Almost all the fluorescence from Cy5-pDNA incorporated into PEG-PAsp(DET) micelles disappeared from the blood 30 min after injection. On the other hand, PEG-PAsp(DET)-Chole micelles retained more than 15% and 2% of the injected dose of pDNA in the blood at 30 min and at 60 min after



**Fig. 11.** Cy5-labeled pDNA concentration in the blood after intravenous injection of PEG-PAsp(DET) (closed bars) and PEG-PAsp(DET)-Chole (open bars) polyplex micelles (N/P = 8, 20 μg pDNA/mouse). Error bars in the graph represent SEM, n = 4. \**P* < 0.05 and \*\**P* < 0.01.

injection, respectively. PEG-PAsp(DET)-Chole micelles could hold pDNA more stably in the blood compared to PEG-PAsp(DET) micelles, probably due to their higher stability in proteinous medium (Fig. 5).

### 3.13. Anti-tumor activity

Polyplex micelles containing sFlt-1 pDNA were injected intravenously into mice-bearing pancreatic adenocarcinoma BxPC3, followed by evaluation of tumor volume (Fig. 12). sFlt-1, which is a soluble form of VEGF receptor-1, is a well-known anti-angiogenic protein [21,22]. We recently reported that systemic injection of polyplex micelles containing sFlt-1 pDNA into mice significantly decreased subcutaneously inoculated BxPC3 growth [16,23], and therefore, this subcutaneous BxPC3 model is appropriate to evaluate the performance of systemic gene delivery vectors. PEG-PAsp(DET) ( $N/P = 10$  and  $20$ ) and PEG-PAsp(DET)-Chole ( $N/P = 15$ ) micelles were administered every four days for three total doses, i.e. on days 0, 4, and 8. Only the PEG-PAsp(DET)-Chole micelle significantly suppressed tumor growth compared to Hepes buffer (control) ( $P < 0.05$ ).

## 4. Discussion

PEG-PAsp(DET) micelles are promising gene delivery vectors due to their high transfection ability with low cytotoxicity, however, they must be prepared at high  $N/P$  ratio to achieve high

transfection efficiency [11,13–15,24]. In general, gene vectors internalized into the cells must escape from the endosome prior to enzymatic degradation in lysosome vesicles for efficient transfection. PAsp(DET) polyocations enabled effective escape from the endosome into cytoplasm due to their pH-selective membrane destabilization [12], and thus, a certain amount of PAsp(DET) should be contained within the same endosomal compartment with pDNA to facilitate release. PEG-PAsp(DET) micelles are needed to be prepared at  $N/P > 20$  for effective *in vitro* transfection [11]. In this regard, we showed that almost all the PEG-PAsp(DET) polymers added at  $N/P \geq 4$ , where they may form stoichiometric charged polyplex micelles with pDNA, existed as free polymers by ultracentrifugation analysis (Fig. 1A). Therefore, a large fraction of PEG-PAsp(DET) polymers present in micelle solutions prepared at high  $N/P$  ratios are not associated with pDNA in the culture medium but still assist in the endosomal escape of polyplex micelles. Indeed, the transfection efficiency of pDNA micelles prepared with PEG-PAsp(DET) increased with simultaneous addition of free polymer with micelle solution prepared at  $N/P = 4$  to the cell culture medium (open circles in Fig. 1B), whereas similar transfection efficiency (closed circles in Fig. 1B) was observed with PEG-PAsp(DET) micelle solutions prepared at higher  $N/P$  ratios (which corresponded to the same amount of free polymer added to culture medium in the experiments with micelle solutions prepared at a constant  $N/P$  value of 4). This result indicates that the amount of free polymer in the culture medium is important for improved transfection efficiency, which is consistent with the above-mentioned hypothesis.

In this study, a hydrophobic cholesterol moiety was introduced into the  $\omega$ -terminus of the PAsp(DET) segment of PEG-PAsp(DET) block copolymer for the purpose of achieving sufficient gene transfer at low  $N/P$  ratio and under dilute conditions, thus further developing PEG-PAsp(DET) micelles towards *in vivo* systemic vectors (Scheme 1). PEG-PAsp(DET)-Chole was designed to increase the association number of block copolymers with polyplex micelles by exploiting the hydrophobic nature of cholesterol, which possesses high self-associating ability, to form polyplex micelles over the stoichiometric charge ratio. Indeed, quantification of free polymer in micelle solutions by ultracentrifugation revealed that the number of PEG-PAsp(DET) associating with a pDNA did not change at  $N/P \geq 4$  ( $N^+/P \geq 2$ ) and that polymer added over  $N/P = 4$  existed as free polymers unassociated with pDNA. On the other hand, PEG-PAsp(DET)-Chole micelles prepared at  $N/P \geq 2$  ( $N^+/P \geq 1$ ) showed an increase in the number of polymers associated with pDNA with increased  $N/P$  ratio (Fig. 4A). Furthermore, the introduction of cholesterol contributed not only to the enhancement of associating ability of polymers to pDNA, but also increased the stability of polyplex micelles. PEG-PAsp(DET)-Chole micelles maintained their structure for 12 h in the presence of BSA with no change in their initial size and PDI (Fig. 5). Note that a stability of a gene delivery vector against serum proteins is an important factor for *in vitro* transfection in the presence of serum and also for *in vivo* transfection via systemic administration and exposure to complex biological milieu in blood. Uptake of pDNA incorporating micelles in culture cells was drastically increased by the introduction of cholesterol (Fig. 8A), likely due to the increased stability of polyplex micelles in the culture medium containing serum. With respect to block copolymer uptake (in experiments performed with micelle solutions prepared with fluorescent-labeled block copolymer), PEG-PAsp(DET)-Chole was internalized into Huh-7 cells significantly more than PEG-PAsp(DET), implying that their uptake is enhanced when associated with polyplex micelles. CLSM observation of the intracellular distribution of polyplex micelles in culture cells revealed that PEG-PAsp(DET)-Chole micelles could more effectively escape from the late endosome/lysosome

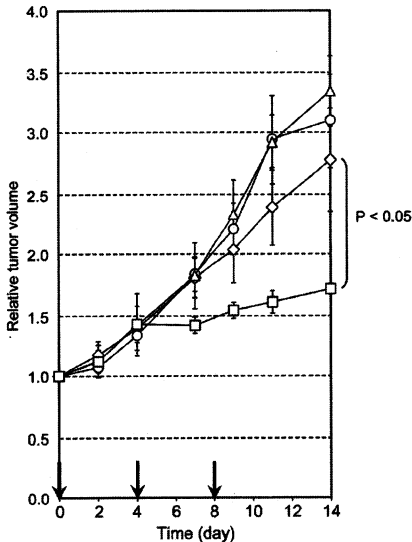


Fig. 12. Anti-tumor activity after intravenous injection of Hepes (diamonds), PEG-PAsp(DET) polyplex micelles at  $N/P = 10$  (circles), at  $N/P = 20$  (triangles), and PEG-PAsp(DET)-Chole polyplex micelles at  $N/P = 15$  (squares). Error bars in the graph represent SEM,  $n = 4$ .

compartments compared to PEG-PAsp(DET) micelles prepared at the same N/P ratio (Fig. 9). In order for polyplex micelles based on the PEG-PAsp(DET) to be effective gene delivery vectors, block copolymer should be released from polyplex micelles in the endosome and the directly associate with the endosomal membrane to disrupt the vesicle structure and facilitate escape of polyplex micelles into the cytoplasm and allow pDNA to further transport into the nucleus. The relative number of PEG-PAsp(DET)-Chole polymers associating with pDNA estimated by FCS measurement was significantly reduced with decreasing pH, from 42% (pH 7.3) to 24% (pH 5.5) (Fig. 10B). These results suggest that formation of PEG-PAsp(DET)-Chole micelles over stoichiometric charge ratio facilitated effective detachment of block copolymers from polyplex micelles in the acidic endosome by electrostatic repulsion among block copolymers, resulting in efficient endosomal escape based on destabilization of the endosomal membrane. Transfection experiments performed *in vitro* revealed that PEG-PAsp(DET)-Chole micelles achieved high transfection efficiency at lower N/P ratios compared to PEG-PAsp(DET) micelles (Fig. 6A). This enhanced transfection ability is likely due to a synergistic effect between effective uptake of pDNA by increased micelle stability, the ability to form micelles with high polymer association above the stoichiometric N/P value, and efficient endosomal escape by polymers released from the micellar structure upon acidification without increased cytotoxicity, even at high N/P ratios (Fig. 6B).

Gene delivery vectors administered systemically are diluted instantly upon injection, and cannot always reach target sites in high concentration. Therefore, systemic gene vectors must transfect efficiently even under dilute conditions. In this regard, PEG-PAsp(DET)-Chole micelles were confirmed to overcome this issue (Fig. 7). Furthermore, whereas the *in vitro* transfection efficiency of PEG-PAsp(DET) micelles dropped dramatically with decreasing pDNA concentration contained in the culture medium, a decrease in transfection efficiency of PEG-PAsp(DET)-Chole micelles was well prevented. This result corroborates well with the results of FCS measurement of micelle solutions (Fig. 10A), which revealed that the diffusion time of PEG-PAsp(DET)-Chole micelles was not changed by dilution, suggesting that their association state was not altered. The inherent characteristics of PEG-PAsp(DET)-Chole micelles, i.e., high transfection efficiency both at low N/P ratios and under dilute conditions, should be suitable for their use as systemic gene delivery vectors.

The increased stability of polyplex micelles was also confirmed by evaluation of blood circulation after systemic injection into mice via the tail vein (Fig. 11). Naked pDNA is not stable in blood and is reported to be degraded within 5 min after intravenous injection [25]. Although pDNA loaded PEG-PAsp(DET) micelles retained more than 20% of injected dose after 15 min, almost all the pDNA were cleared from the blood after 30 min (Fig. 11). PEG-PAsp(DET) micelles are known to easily decondense in the presence of serum [20], thus, PEG-PAsp(DET) micelles injected directly into the blood stream are likely to decondense and release pDNA, which is subsequently degraded and removed from circulation. On the other hand, PEG-PAsp(DET)-Chole micelles showed significantly prolonged blood circulation compared to PEG-PAsp(DET) micelles (Fig. 11). PEG-PAsp(DET)-Chole micelles, which were stable in the presence of BSA (Fig. 5), likely resist rapid decondensation, leading to longer circulation time.

Polyplex micelles were further evaluated for anti-tumor activity against a murine solid tumor model after intravenous injection in order to evaluate their performance as systemic gene delivery vectors (Fig. 12). Specifically, mice bearing a subcutaneously xenografted BxPC3 human pancreatic adenocarcinoma tumor and therapeutic pDNA encoding the anti-angiogenic protein sFlt-1 were

used. As shown in Fig. 12, PEG-PAsp(DET) micelles showed no significant effect, however, PEG-PAsp(DET)-Chole micelles significantly suppressed tumor growth compared to the Hepes buffer control. Important factors affecting the anti-tumor effect of systemically injected gene delivery vectors are stability in the blood and high transfection efficiency within cells at the target site [16]. PEG-PAsp(DET)-Chole micelles exhibited longer blood circulations (Fig. 11) and also maintained high transfection ability even under dilute conditions (Fig. 7) compared to PEG-PAsp(DET) micelles, which correlated to higher therapeutic effect *in vivo*.

## 5. Conclusion

PEG-PAsp(DET) micelles achieve high transfection efficiency with low cytotoxicity at high N/P ratios, however, the results of this work showed that block copolymer added over the stoichiometric charge ratio exists as free polymers in the micelles solution. In this study, we further improved the design of PEG-PAsp(DET)-based synthetic gene delivery vectors by incorporating a cholesterol moiety into the terminus of PAsp(DET) segment in the block copolymer. PEG-PAsp(DET)-Chole micelles could be formed over the stoichiometric charge ratio due to self-association of cholesterol, and achieved effective endosomal escape due to the efficient delivery of block copolymers and pDNA into target cells and which increased transfection efficiency at low N/P ratios and under the dilute conditions. Furthermore, cholesterol introduction led to increased stability of polyplex micelles in the blood, which resulted in significant suppression of subcutaneous pancreatic tumor growth by intravenous injection of polyplex micelles loading sFlt-1 pDNA. Conventional polyplexes formed with polyethylenimine or cationic polypeptides have similar issues regarding the impact of free polycations on transfection efficiency as observed with PEG-PAsp(DET) micelles [26,27]. These polyplexes must be used at high N/P ratio or high concentration of pDNA to achieve effective endosomal escape and high transfection efficiency. Thus, the large amount of free polymer can result in increased cytotoxicity *in vitro* and also adverse side effects *in vivo* after intravenous injection. To circumvent the issue of excess polycations not associating with pDNA, polyplexes utilizing hydrophobic groups such as cholesterol have been reported [28,29] and such systems show promise due to excellent transfection efficiency. Nevertheless, those studies focused primarily on increased stability of polyplexes by introduction of cholesterol, with less attention paid to the association number of polymers with polyplexes. In this study, we showed that PEG-PAsp(DET)-Chole micelles with high polymer association could be formed over the stoichiometric charge ratio by detailed evaluation of micelle solutions using ultracentrifugation analysis. Enhanced stability as well as complex formation over the stoichiometric charge ratio contributed to effective gene transfection both *in vitro* and *in vivo*. These findings are extremely helpful for design of non-viral gene vectors and represent a significant improvement towards the use of synthetic polyplex micelle gene delivery vectors as a practical therapeutic modality.

## Acknowledgements

This work was financially supported by the Core Research Program for Evolutional Science and Technology (CREST) from Japan Science and Technology Agency (JST) as well as by Grants-in-Aid for Young Scientists (A) (No. 20689024 to M.O.). We express our appreciation to Prof. Masabumi Shibuya (Tokyo Medical and Dental University) for providing pVL 1393 baculovirus vector pDNA encoding human sFlt-1. We thank Ms. Junko Kawakita and Ms. Satomi Ogura (The University of Tokyo) for technical assistance.

## Appendix

Figures with essential color discrimination. Fig. 9 in this article may be difficult to interpret in black and white. The full color images can be found in the on-line version, at doi:10.1016/j.biomaterials.2010.09.022.

## References

- Mastroianni E, van der Aa MAEM, Hennink WE, Crommelin DJA. Artificial viruses: a nanotechnological approach to gene delivery. *Nat Rev Drug Discov* 2006;5:115–21.
- Mintzer M, Simanek EE. Nonviral vectors for gene delivery. *Chem Rev* 2009;109:259–302.
- Kakizawa Y, Kataoka K. Block copolymer micelles for delivery of gene and related compounds. *Adv Drug Deliv Rev* 2002;54:203–22.
- Merdan T, Kopecek J, Kissel T. Prospects for cationic polymers in gene and oligonucleotide therapy against cancer. *Adv Drug Deliv Rev* 2002;54:715–58.
- Pack DW, Hoffman AS, Pun S, Stayton PS. Design and development of polymers for gene delivery. *Nat Rev Drug Discov* 2005;4:581–93.
- Kataoka K, Togawa H, Harada A, Yasugi K, Matsumoto T, Katayose S. Spontaneous formation of polyion complex micelles with narrow distribution from antisenescence oligonucleotide and cationic block copolymer in physiological saline. *Macromolecules* 1996;29:8556–7.
- Katayose S, Kataoka K. Water-soluble polyion complex associates of DNA and poly(ethylene glycol)-poly(L-lysine) block copolymer. *Bioconjug Chem* 1997;8:702–7.
- Kabanov AV, Kabanov VA. Interpolyelectrolyte and block ionomer complexes for gene delivery: physicochemical aspects. *Adv Drug Deliv Rev* 1998;30:49–60.
- Osada K, Christie JR, Kataoka K. Polymeric micelles from poly(ethylene glycol)-poly(amino acid) block copolymer for drug and gene delivery. *J R Soc Interface* 2009;6:S325–39.
- Itaka K, Kataoka K. Recent development of nonviral gene delivery systems with virus-like structures and mechanism. *Eur J Pharm Biopharm* 2009;71:475–83.
- Kanayama N, Fukushima S, Nishiyama N, Itaka K, Jang WD, Miyata K, et al. A PEG-based biocompatible block cationomer with high buffering capacity for the construction of polyplex micelles showing efficient gene transfer toward primary cells. *Chem Med Chem* 2006;1:439–44.
- Miyata K, Oba M, Nakanishi M, Fukushima S, Yamasaki Y, Koyama H, et al. Polyplexes from poly(aspartamide) bearing 1,2-diaminoethane side chains induce pH selective, endosomal membrane destabilization with amplified transfection and negligible cytotoxicity. *J Am Chem Soc* 2008;130:16287–94.
- Akagi D, Oba M, Koyama H, Nishiyama N, Fukushima S, Miyata T, et al. Biocompatible micellar nanovectors achieve efficient gene transfer to vascular lesions without cytotoxicity and thrombus formation. *Gene Ther* 2007;14:1029–38.
- Itaka K, Ohba S, Miyata K, Kawaguchi H, Nakamura K, Takato T, et al. Bone regeneration by regulated in vivo gene transfer using biocompatible polyplex nanomicelles. *Mol Ther* 2007;15:1655–62.
- Harada-Shiba M, Takamisawa I, Miyata K, Ishii T, Nishiyama N, Itaka K, et al. Intratracheal gene transfer of adrenomedullin using polyplex nanomicelles attenuates monocrotaline-induced pulmonary hypertension in rats. *Mol Ther* 2009;17:1180–6.
- Oba M, Vachutinsky Y, Miyata K, Kano MR, Ikeda S, Nishiyama N, et al. Antiangiogenic gene therapy of solid tumor by systemic injection of polyplex micelles loading plasmid DNA encoding soluble Flt-1. *Mol Pharmaceutics* 2010;7:501–9.
- Oba M, Aoyagi K, Miyata K, Matsumoto Y, Itaka K, Nishiyama N, et al. Polyplex micelles with cyclic RGD peptide ligands and disulfide cross-links directing to the enhanced transfection via controlled intracellular trafficking. *Mol Pharmaceutics* 2008;5:1080–92.
- Nakanishi M, Park JS, Jang WD, Oba M, Kataoka K. Study of the quantitative aminolysis reaction of poly( $\beta$ -benzyl L-aspartate) (PBLA) as a platform polymer for functionality materials. *React Funct Polym* 2007;67:1361–72.
- Takae S, Miyata K, Oba M, Ishii T, Nishiyama N, Itaka K, et al. PEG-detachable polyplex micelles based on disulfide-linked block cationomers as bioresponsive nonviral gene vectors. *J Am Chem Soc* 2008;130:6001–9.
- Miyata K, Fukushima S, Nishiyama N, Yamasaki Y, Kataoka K. PEG-based block cationomers possessing DNA anchoring and endosomal escaping functions to form polyplex micelles with improved stability and high transfection efficacy. *J Control Release* 2007;122:252–60.
- Shibuya M, Yamaguchi S, Yamane A, Ikeda T, Tojo A, Matsumine H, et al. Nucleotide sequence and expression of a novel human receptor-type tyrosine kinase gene (flt) closely related to the fms family. *Oncogene* 1990;5:519–24.
- Kendall RL, Thomas KA. Inhibition of vascular endothelial cell growth factor activity by an endogenously encoded soluble receptor. *Proc Natl Acad Sci U S A* 1993;90:10705–9.
- Vachutinsky Y, Oba M, Miyata K, Hiki S, Kano MR, Nishiyama N, et al. Antiangiogenic gene therapy of experimental pancreatic tumor by sFlt-1 plasmid DNA carried by RGD-modified crosslinked polyplex micelles. *J Control Release* (in press).
- Han M, Bae Y, Nishiyama N, Miyata K, Oba M, Kataoka K. Transfection study of using multicellular tumor spheroids for screening non-viral polymeric gene vectors with low cytotoxicity and high transfection efficiencies. *J Control Release* 2007;121:38–48.
- Harada-Shiba M, Yamauchi K, Harada A, Takamisawa I, Shimokado K, Kataoka K. Polyion complex micelles as vectors in gene therapy-pharmacokinetics and in vivo gene transfer. *Gene Ther* 2001;9:407–14.
- Boeckle S, von Cersdorff K, van der Piepen S, Cuijse C, Wagner E, Ogris M. Purification of polyethylenimine polyplexes highlights the role of free poly-cations in gene transfer. *J Gene Med* 2004;6:1102–11.
- Fahrmeir J, Gunther M, Tietze N, Wagner E, Ogris M. Electrophoretic purification of tumor-targeted polyethylenimine-based polyplexes reduces toxic side effects in vivo. *J Control Release* 2007;122:236–45.
- Han SO, Mahato RI, Kim SW. Water-soluble lipopolymer for gene delivery. *Bioconjug Chem* 2001;12:337–45.
- Guo XD, Tandiono F, Wiradharma N, Khor D, Tan CG, Khan M, et al. Cationic micelles self-assembled from cholesterol-conjugated oligopeptides as an efficient gene delivery vector. *Biomaterials* 2008;29:4838–46.

## DRUG DELIVERY

## Improving Drug Potency and Efficacy by Nanocarrier-Mediated Subcellular Targeting

Mami Murakami,<sup>1</sup> Horacio Cabral,<sup>1,2</sup> Yu Matsumoto,<sup>3</sup> Shourong Wu,<sup>3</sup> Mitsunobu R. Kano,<sup>4</sup> Takao Yamori,<sup>5</sup> Nobuhiro Nishiyama,<sup>2,3\*</sup> Kazunori Kataoka<sup>1,2,3,6\*</sup>

Nanocarrier-mediated drug targeting is an emerging strategy for cancer therapy and is being used, for example, with chemotherapeutic agents for ovarian cancer. Nanocarriers are selectively accumulated in tumors as a result of their enhanced permeability and retention of macromolecules, thereby enhancing the antitumor activity of the nanocarrier-associated drugs. We investigated the real-time subcellular fate of polymeric micelles incorporating (1,2-diaminocyclohexane) platinum(II) (DACHPt/m), the parent complex of oxaliplatin, in tumor tissues by fluorescence-based assessment of their kinetic stability. These observations revealed that DACHPt/m was extravasated from blood vessels to the tumor tissue and dissociated inside each cell. Furthermore, DACHPt/m selectively dissociated within late endosomes, enhancing drug delivery to the nearby nucleus relative to free oxaliplatin, likely by circumvention of the cytoplasmic detoxification systems such as metallothionein and methionine synthase. Thus, these drug-loaded micelles exhibited higher antitumor activity than did oxaliplatin alone, even against oxaliplatin-resistant tumors. These findings suggest that nanocarriers targeting subcellular compartments may have considerable benefits in clinical applications.

## INTRODUCTION

In 2009, about 10 million people worldwide were newly diagnosed with cancer (1). Application of nanotechnology to cancer therapy may offer therapeutic effects that cannot be achieved with other strategies. The main aim of this approach is to develop noscale drug vehicles for targeted cancer therapy (2–5). Nanocarriers selectively accumulate in solid tumors as a result of the enhanced permeability and retention (EPR) effect, which is characterized by microvascular hyperpermeability to circulating macromolecules and impaired lymphatic drainage in tumor tissues (6). At present, several nanocarrier formulations have been approved for clinical use against ovarian cancer and HIV-associated Kaposi's sarcoma (Doxil) and breast cancer (Abraxane). These formulations allow better accumulation of the drugs doxorubicin and paclitaxel in tumors (7).

Polymeric micelles, self-assemblies of block copolymers, have gained increasing popularity as tumor-targetable nanocarriers since they were first used as drug vehicles in the late 1980s (8–12). These micelles, which are several tens of nanometers in size and have a characteristic core-shell structure consisting of a drug-loaded hydrophobic core and poly(ethylene glycol) (PEG) hydrophilic shell, are long-lived in the bloodstream and effectively accumulate in solid tumors after intravenous injection (8). The critical features of polymeric micelles for their function as drug vehicles, including size, drug loading and release, and specific binding to the target cells, can be modulated by engineering the

constituent block copolymers. At present, our micelle formulations incorporating doxorubicin, paclitaxel, SN-38, cisplatin, and (1,2-diaminocyclohexane) platinum(II) (DACHPt) are undergoing clinical trials (development code names NK911, NK105, NK012, NC-6004, and NC-4016, respectively), and four of these have advanced to Phase II studies (13–17). These clinical studies have revealed that polymeric micelles reduce side effects from the incorporated drugs and are effective against various intractable tumors, such as triple-negative breast cancers (18), indicating their clinical potential.

Recently, increasing attention has been paid to another potentially useful property of nanocarriers: to achieve subcellular drug targeting. Subcellular drug targeting of nanocarriers could enhance the pharmacological activity of the loaded drugs through improved subcellular drug distribution (19). Drug vehicles designed to release active drugs in acidic organelles, such as the endosome and lysosome, can circumvent recognition by the drug efflux pump (for example, P-glycoprotein) through internalization by endocytosis, thus overcoming multidrug resistance in cancer cells (20–22). Here, we aimed to investigate the potential of DACHPt-loaded micelles (DACHPt/m) for *in vivo* subcellular targeting. DACHPt/m is formed by the polymer-metal complexation between DACHPt and the carboxylic group of poly(ethylene glycol)-*b*-poly(glutamic acid) [PEG-*b*-P(Glu)] copolymers. DACHPt is the parent complex of the clinically approved drug oxaliplatin. Oxaliplatin has a hydrolyzable oxalate group to increase its solubility in water, which can be removed by nucleophiles in biological media, such as chloride ions. Aqua complexes ( $[(\text{DACH})\text{Pt}(\text{H}_2\text{O})\text{Cl}]^+$  or  $[(\text{DACH})\text{Pt}(\text{H}_2\text{O})_2]^{2+}$ ) of DACHPt exhibit chemotherapeutic activity. DACHPt/m releases DACHPt and the micelle structure dissociates depending on the pH and chloride ion concentrations, a result of ligand substitution of the Pt(II) from the carboxylates in the micelle core with the chloride ions in the medium (Fig. 1A) (23, 24). Moreover, after DACHPt/m is internalized into cancer cells, it would be expected to be exposed to different pH and chloride ion concentrations during subcellular trafficking (25). We hypothesized that DACHPt/m would be selectively released in low-pH cellular compartments, bypassing

<sup>1</sup>Department of Bioengineering, Graduate School of Engineering, University of Tokyo, 7-3-1 Hongo, Bunkyo-ku, Tokyo 113-8656, Japan. <sup>2</sup>Center for NanoBio Integration, University of Tokyo, Tokyo 113-8656, Japan. <sup>3</sup>Center for Disease Biology and Integrative Medicine, Graduate School of Medicine, University of Tokyo, Tokyo 113-0033, Japan. <sup>4</sup>Department of Molecular Pathology, Graduate School of Medicine, University of Tokyo, Tokyo 113-0033, Japan. <sup>5</sup>Division of Molecular Pharmacology, Cancer Chemotherapy Center, Japanese Foundation for Cancer Research, 3-10-6 Ariake, Koto-ku, Tokyo 135-8550, Japan. <sup>6</sup>Department of Materials Engineering, Graduate School of Engineering, University of Tokyo, Tokyo 113-8656, Japan.

\*To whom correspondence should be addressed. E-mail: nishiyama@bmv.tu.tyoto.ac.jp (NN); kataoka@bmv.tu.tyoto.ac.jp (KK)

cytoplasmic detoxification and thereby improving potency and efficacy (Fig. 1B). Indeed, we previously reported that cisplatin-loaded micelles, which are formed in the same manner as DACHPt/m, caused different gene expression patterns than did cisplatin alone because of their different internalization pathways and the facilitated drug release in endosomes and lysosomes (26). To test the above-mentioned hypothesis, we constructed fluorescent-labeled DACHPt/m (F-DACHPt/m) with a dual fluorescent-labeling method so that we could follow the intracellular localization and dissociation of the micelles by using *in vivo* confocal microscopy, and intravitally evaluated the extravasation, penetration, cellular uptake, and subcellular fate of DACHPt/m in tumor tissues and their activity against human colorectal cancers.

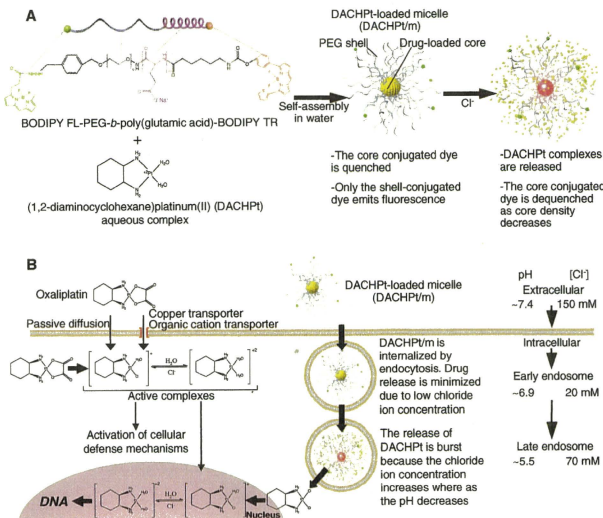
## RESULTS

### Construction and characterization of F-DACHPt/m

To construct the dual fluorescent-labeled block copolymer, we conjugated the fluorescent dyes boron dipyrromethene (BODIPY) FL (excitation wavelength, 503 nm; emission wavelength, 512 nm) and BODIPY TR (excitation wavelength, 588 nm; emission wavelength, 616 nm) to the  $\alpha$ - and  $\omega$ -end groups of  $\alpha$ -4-(diethoxymethyl)benzyl-poly(ethylene glycol)-*b*-poly(L-glutamic acid), respectively, and thus obtained BODIPY FL-PEG-*b*-P(Glu)-BODIPY TR (fig. S1). The conjugation degree for BODIPY FL to the block copolymer was 0.2 mol BODIPY FL per mole of polymer and for BODIPY TR was about 0.8 mol BODIPY TR per mole of polymer. We built F-DACHPt/m by the formation of polymer-metal complexes between DACHPt and the carboxylic groups of

poly(glutamic acid) in BODIPY FL-PEG-*b*-P(Glu)-BODIPY TR (Fig. 1A). F-DACHPt/m had a diameter of 30 nm, similar to that of DACHPt/m (fig. S2). The intact F-DACHPt/m emitted fluorescence only from the shell-conjugated dye (BODIPY FL) because the core-conjugated dye (BODIPY TR) was quenched owing to its high local concentration. The close proximity of BODIPY TR fluorophores in the core of the micelles leads to self-quenching by the formation of nonfluorescent ground-state BODIPY TR dimers (or higher aggregates) (27). When DACHPt is released as a result of the ligand substitution of the Pt(II) from the carboxylates in the micelle core with the chloride in the medium, the density of the micelle core is reduced and the fluorescence of BODIPY TR is dequenched (Fig. 1A). We investigated the release of DACHPt from F-DACHPt/m and the fluorescence of BODIPY FL and BODIPY TR at the surface and core of the micelles, respectively, under conditions that mimicked the extracellular medium (pH 7.4 and 150 mM Cl<sup>-</sup>), early endosomes (pH 6.9 and 20 mM Cl<sup>-</sup>), and late endosomes and lysosomes (pH 5.5 and 70 mM Cl<sup>-</sup>) (25). The fluorescence from BODIPY FL on the shell of the micelles was constant regardless of the pH and salt concentration of the media (Fig. 2, A to C, middle columns), suggesting that the fluorescence from BODIPY FL can be used to trace the position of the micelles in the biological environment. In addition, the drug release profile of F-DACHPt/m was similar to that of unmodified DACHPt/m, suggesting the feasibility of a direct comparison (Fig. 2, A to C, left columns). Under extracellular conditions, BODIPY TR fluorescence increased after an incubation period of 17 hours, simultaneous with the release of DACHPt from F-DACHPt/m (Fig. 2A). The release of DACHPt from F-DACHPt/m in the late endosomal conditions was considerably faster (Fig. 2C) than in the extra-

**Fig. 1.** Design of fluorescent-labeled DACHPt/m (F-DACHPt/m) for visualization of the localization and drug release in the cell. (A) F-DACHPt/m self-assembled through polymer-metal complex formation between DACHPt and boron dipyrromethene (BODIPY) FL-poly(ethylene glycol)-*b*-poly(glutamic acid)-BODIPY TR in distilled water. In the micelle state, only BODIPY FL (green) emits fluorescence, whereas BODIPY TR (red) remains quenched. As DACHPt is released from F-DACHPt/m in chloride ion-containing media, BODIPY TR is dequenched and emits fluorescence. (B) Schematic representation of hypothetical subcellular pathways and action of DACHPt/m. Oxaliplatin enters cells by passive diffusion or through copper/organic cation transporters. Once oxaliplatin is in the cytoplasm, most of the activated aqua species ([DACHPt(H<sub>2</sub>O)Cl<sup>+</sup>] or [DACHPt(H<sub>2</sub>O)<sub>2</sub>]<sup>2+</sup>) are eliminated by cellular detoxification mechanisms, but a small fraction binds to DNA. In contrast, DACHPt/m that enters tumor cells by endocytosis (middle) is exposed to an environment with increasing acidity and chloride ion concentration because early endosomes mature into the late endosomes. Drug release from DACHPt/m is accelerated in the late endosomal environment close to the perinuclear region, resulting in enhanced efficiency of drug delivery to the nucleus.



cellular and early endosomal conditions (Fig. 2, A and B), occurring without any delay. Further, mirroring the DACHPt release, F-DACHPt/m exhibited more robust fluorescence recovery of BODIPY TR under the late endosomal conditions (Fig. 2C) than under the early endosomal conditions (Fig. 2B, right columns). Thus, the fluorescence profiles of BODIPY TR are correlated with the release profiles of DACHPt from the micelles.

### In vitro subcellular trafficking of F-DACHPt/m

The cellular internalization and fate of F-DACHPt/m in human tumor-derived colorectal cancer (HT29) cells, which are the most frequently used cell lines in oxaliplatin studies (28), were observed with time-lapse confocal laser scanning microscopy (CLSM) (Fig. 3A and video S1). The intensity of BODIPY FL fluorescence increased slightly over time (Fig. 3B), and the BODIPY FL fluorescence in the images was clearly visible within a 6-hour incubation (Fig. 3A). Meanwhile, with time,

the intensity of BODIPY TR fluorescence continuously increased to a greater extent than did that of BODIPY FL fluorescence (Fig. 3B), and the BODIPY TR fluorescence in the images became visible at about 24 hours of incubation (Fig. 3A). This continuous increase in the intensity of BODIPY TR fluorescence corresponds to the quenching of BODIPY TR fluorescence driven by the release of DACHPt in the cell. These results suggest that F-DACHPt/m enters the cells as a micelle form and then dissociates within the subcellular environments.

Using CLSM with higher magnification, we further evaluated the detailed subcellular trafficking and fate of F-DACHPt/m by focusing on individual cells. We confirmed that the micelles entered the cancer cells via endocytosis by incubating the cells with F-DACHPt/m at 37°C and 4°C. As endocytosis ceases at 4°C, the fluorescent signal of F-DACHPt/m inside the cells was undetectable, whereas at 37°C, the fluorescence from F-DACHPt/m was observed inside the cells (fig. S3). To examine the

subcellular trafficking of the micelles, we determined the colocalization of BODIPY FL fluorescence from F-DACHPt/m with an early endosome marker, Rab5a-RFP and a late endosome and lysosome marker, LysoTracker, in HT29 cells (Fig. 3C). Note that individual vesicular organelles can be recognized as punctate fluorescence in the images. After a 6-hour incubation at 37°C, BODIPY FL colocalized mainly with Rab5a-RFP (yellow fluorescence in Fig. 3C, upper images) rather than with LysoTracker. After prolonged incubation (24 and 55 hours), BODIPY FL showed decreased colocalization with Rab5a-RFP and increased colocalization with LysoTracker (yellow fluorescence in Fig. 3C, lower images). This observation was confirmed by quantification of colocalized fluorescent intensities of BODIPY FL with Rab5a-RFP or LysoTracker (Fig. 3D). These results suggested that the micelles might localize mainly in the early endosome until 6 hours and then move into the late endosome/lysosome compartment. Furthermore, we studied the timing and location of the micelle dissociation and concomitant drug release by evaluating the colocalization of F-DACHPt/m with LysoTracker (Fig. 3E and fig. S4A) and the quantification of BODIPY FL and BODIPY TR fluorescent intensities (fig. S4B), as well as the colocalization ratio (Fig. 3F). The fluorescence intensity from BODIPY FL gradually increased (fig. S4B). Meanwhile, the fluorescence of BODIPY TR became visible after 24-hour incubation (Fig. 3E and fig. S4A) and then increased over time (fig. S4B). Both BODIPY FL and BODIPY TR colocalized with LysoTracker (Fig. 3E and fig. S4A), and the colocalization ratio between BODIPY FL or BODIPY TR and LysoTracker increased over time (Fig. 3F). These observations sug-

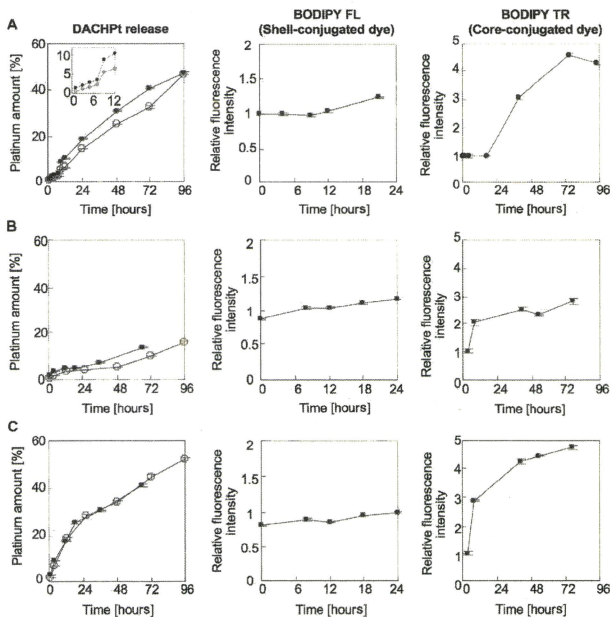


**Fig. 2.** Properties of F-DACHPt/m under conditions mimicking extracellular and subcellular environments. (A to C) Release profiles of DACHPt from DACHPt/m and F-DACHPt/m (left column) and fluorescence profiles of BODIPY FL (middle column) and BODIPY TR (right column) under conditions mimicking (A) the extracellular environment (10 mM PBS, pH 7.4, and 150 mM NaCl), (B) the early endosomal environment (10 mM PBS, pH 6.9, and 20 mM NaCl), and (C) the late endosomal environment (10 mM PBS, pH 5.5, and 70 mM NaCl), all at 37°C. Inset in top left panel is the magnification of the profiles of DACHPt release until 12 hours. The release of DACHPt from the micelles was evaluated by dialysis as described in Materials and Methods. Data for DACHPt and F-DACHPt/m in the left column are shown as open and filled circles, respectively. Data are expressed as means  $\pm$  SEM ( $n = 3$ ).

gested that F-DACHP/m progressively dissociated in the late endosome and lysosomal compartments. Because these acidic organelles reside in the perinuclear region, F-DACHP/m would be expected to deliver the active platinum complexes close to the nucleus. Thus, *in vitro* confocal microscopy revealed that F-DACHP/m appears to exhibit late endosome/lysosome-selective dissociation concomitant with the release of DACHPt, thereby achieving efficient DACHPt delivery close to the nucleus.

**Effect of subcellular pathway on drug efficiency**

Oxaliplatin enters the cells by passive diffusion or through copper/organic cation transporters (29), and it then changes to active DACHPt aqua complexes in the cytoplasm, some of which may ultimately cross-link with DNA, disrupting DNA function and exerting therapeutic activity (Fig. 1B). However, 75 to 85% of activated platinum drugs are sequestered by abundant sulfur species that serve as cellular defense mechanisms in the cytoplasm, and only 5 to 10% of oxaliplatin can bind to DNA (Fig. 1B) (30–32). We hypothesized that DACHP/m facilitates drug delivery close to the nucleus through its perinuclear subcellular localization. Therefore, we studied the pharmacological activity of DACHP/m. DACHP/m displayed a value of  $IC_{50}$  (the mean concentration that causes 50% growth inhibition) against HT29 cells that was lower than that of oxaliplatin by a factor of 4.7 (Table 1). It is rare that a nanocarrier-encapsulated drug surpasses the free form of the drug for *in vitro* cytotoxicity (33). To elucidate the mechanism of DACHP/m action, we evaluated the subcellular accumulation of platinum and quantity of Pt-DNA adducts. Exposure of HT29 cells to oxaliplatin resulted in twice as much accumulation of platinum than did exposure to DACHP/m (Fig. 3G). This is probably because oxaliplatin rapidly enters the cells by diffusion and through copper/organic cation transporters (29), whereas DACHP/m is gradually internalized by endocytosis. Nevertheless, we did not observe a significant difference in the Pt-DNA adducts formed after exposure to oxaliplatin and DACHP/m (Fig. 3H), indicating that DACHP/m may efficiently deliver the active platinum drug to DNA (Fig. 3I).

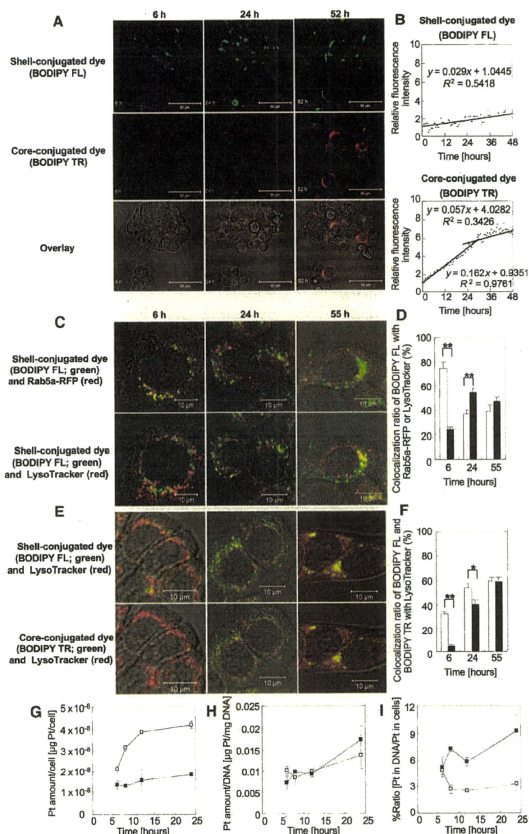


**Fig. 3.** *In vitro* observation of subcellular trafficking and fate of F-DACHP/m, cellular platinum accumulation, and formation of platinum-DNA adducts. (A) Representative images of time-lapse CLSM observation of HT29 cells treated with F-DACHP/m (green, BODIPY FL; red, BODIPY TR; yellow, their colocalization). (B) Relative fluorescence intensity of BODIPY FL (upper) and BODIPY TR (lower) of F-DACHP/m. (C) Fluorescent images of colocalization of BODIPY FL of DACHP/m (green) with an early endosome marker, Rab5a-RFP (red in upper images), or a late endosome and lysosome marker, LysoTracker (red in lower images), in HT29 cells after incubation for 6, 24, and 55 hours. (D) Colocalization ratio of BODIPY FL with Rab5a-RFP (open bars) or LysoTracker (closed bars). Data are expressed as means  $\pm$  SEM ( $n = 10$ ),  $**P < 0.01$ . (E) Fluorescent images of colocalization of BODIPY FL (green in upper images) and BODIPY TR (green in lower images) of F-DACHP/m with LysoTracker (red) in HT29 cells after incubation for 6, 24, and 55 hours. (F) Colocalization ratio of BODIPY FL (open bars) or BODIPY TR (closed bars) with LysoTracker. Data are expressed as means  $\pm$  SEM ( $n = 10$ ),  $*P < 0.05$ ;  $**P < 0.01$ . (G) *In vitro* cellular accumulation of platinum. (H) DNA platinumation. (I) Ratio of platinum in DNA to total platinum in cells expressed as a percentage. DNA platinumation was converted from  $\mu\text{g Pt/mg DNA}$  to  $\mu\text{g Pt/cell}$ , and the ratio was calculated. Open squares, oxaliplatin; filled squares, DACHP/m. Data are expressed as means  $\pm$  SEM ( $n = 3$ ).



We also evaluated the mean concentration required for 50% growth inhibition ( $GI_{50}$ ), which is defined as in (34, 35), in a human cell panel composed of 37 cancer cell lines (fig. S5), and investigated the correlation between  $GI_{50}$  and expression of 26 genes that we selected on the basis of their potential association with the pharmacological activity of platinum compounds (36). The cytotoxic activity of oxaliplatin was inversely correlated with the expression of metallothionein (MT1Q) and methionine synthase (MTR), which are found in the cytoplasm and inactivate platinum compounds. DACHPt/m cytotoxicity did not exhibit similar correlations (table S1). We conclude that DACHPt/m may bypass cytoplasmic detoxification by MTR and MT1Q and efficiently deliver active platinum complexes to the nucleus, because they are internalized by endocytosis and selectively release the active platinum complexes in the late endosome/lysosome compartment (Fig. 1B).

### Effect of DACHPt/m on oxaliplatin resistance in vitro

Our proposed mechanism of action of DACHPt/m led us to investigate their efficacy in oxaliplatin-resistant cancer cells, because MTR and MT1Q are overexpressed in these cells (37–39). We developed oxaliplatin-resistant HT29 cells (HT29/ox) by chronic exposure of HT29 cells to oxaliplatin with gradual dose escalation. Relative to the parental HT29 cells, HT29/ox cells were 10 times as resistant to oxaliplatin (Table 1). Quantitative real-time reverse transcription polymerase chain reaction (RT-PCR) and Western blotting revealed that the HT29/ox cells showed up-regulated messenger RNA (mRNA) as well as protein for MTR and MT1Q compared with HT29 cells (Fig. 4, A and B). Moreover, the down-regulation of MT1Q and MTR with small interfering RNA (siRNA) restored the sensitivity of HT29/ox cells to oxaliplatin (fig. S6). In vitro cytotoxicity studies showed that DACHPt/m was 120 times as cytotoxic as oxaliplatin in HT29/ox cells (Table 1). These results suggested that DACHPt/m may overcome acquired resistance to oxaliplatin.

### In vivo intratumoral imaging of F-DACHPt/m in a human colon cancer model

DACHPt/m would need to extravasate, penetrate into the interstitial tissue, and be internalized by cancer cells after systemic administration to exert the in vivo antitumor activity predicted from the results above. We performed real-time intravital observation of the accumulation and subcellular fate of F-DACHPt/m in HT29 xenografts by using in vivo CLSM equipped with a high-speed resonant scanner developed to acquire live tissue images of experimental animals (fig. S7). Immediately after intravenous injection, F-DACHPt/m was observed in the blood vessels of solid tumors (Fig. 5A and video S2). The fluorescence from F-DACHPt/m in the blood vessels corresponded only to that of BODIPY

FL. Even 12 hours later, only BODIPY FL fluorescence was observed flowing in the blood vessels (Fig. 5B and video S3). These observations indicate that F-DACHPt/m stably circulates in the bloodstream while maintaining their micellar structure. Images of tumor tissue revealed the accumulation and dissociation behaviors of F-DACHPt/m (Fig. 5, C and D, and video S3). Two hours after injection, F-DACHPt/m accumulated within the tumor tissue because of the EPR effect and was identified within the cells, whereas BODIPY TR fluorescence remained quenched. BODIPY TR fluorescence gradually appeared inside the cells 4 hours after injection and was clearly visible after 12 hours, indicating the release of DACHPt

**Table 1.** In vitro cytotoxicity of free oxaliplatin and DACHPt/m against HT29 and HT29/ox cells after a 48-hour incubation. Data are expressed as means  $\pm$  SEM ( $n = 4$ ).

Cells	$IC_{50}$ ( $\mu$ M)*		
	Free oxaliplatin	DACHPt/m	Oxaliplatin/DACHPt/m
HT29	2.2 $\pm$ 2.2	0.47 $\pm$ 0.05	4.7
HT29/ox	22.8 $\pm$ 2.6	0.19 $\pm$ 0.11	120
Ratio of HT29/ox/HT29	10.4	0.4	—

\* $IC_{50}$  values obtained from the MTT assay.

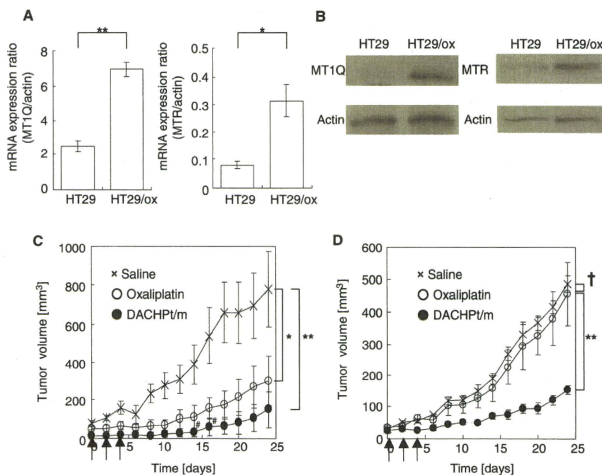


**Fig. 4.** Expression of MT1Q and MTR in HT29/ox cells and effects of DACHPt/m on HT29 and HT29/ox tumors in vivo. (A) Relative mRNA expression of metallothionein (MT1Q) and methionine synthase (MTR) in parent HT29 and HT29/ox cell lines. Data are expressed as means  $\pm$  SEM ( $n = 3$ ). \* $P < 0.05$ ; \*\* $P < 0.01$ . (B) Western blots of MT1Q and MTR in HT29 and HT29/ox cell lines. (C and D) In vivo effect of DACHPt/m on subcutaneous HT29 (C) and HT29/ox (D) tumor cells. Crosses, saline; open circles, oxaliplatin (8 mg/kg); filled circles, DACHPt/m (4 mg/kg); arrows, injection of oxaliplatin and DACHPt/m; †, tumor regression; ‡,  $P > 0.1$ ; \* $P < 0.05$ ; \*\* $P < 0.01$ . Data are expressed as means  $\pm$  SEM ( $n = 4$ ).

from the micelles inside the cells in the tumor tissue. The cell membrane, stained with CellMask, and cell nuclei were substantially free of F-DACHPt/m (Fig. 5, C and D, and video S3). These results were consistent with our *in vitro* results (Fig. 3A) and suggested that F-DACHPt/m percolated into interstitial tissues and was efficiently internalized to endosomal compartments of cells in a micelle form, followed by dissociation of the multimolecular structure of the micelles in the late endosomal and lysosomal compartments.

### DACHPt/m enhances antitumor activity and overcomes oxaliplatin resistance *in vivo*

On the basis of our observations of the *in vivo* behavior of F-DACHPt/m, we hypothesized that DACHPt/m may also overcome oxaliplatin resistance *in vivo*. Thus, we evaluated DACHPt/m *in vivo* antitumor activity against subcutaneous HT29 and HT29/ox tumors (Fig. 4, C and D). Although free oxaliplatin failed to inhibit the growth of HT29/ox tumors, DACHPt/m exhibited substantial antitumor activity in the oxaliplatin-resistant xenograft model and successfully overcame the oxaliplatin resistance of HT29/ox cells *in vivo* (Fig. 4D). Note that DACHPt/m also achieved higher antitumor activity than oxaliplatin against the HT29 tumors (Fig. 4C). Thus, our micelle-based drug delivery vehicle was able to circumvent the detoxification mechanisms against platinum drugs in tumor cell cytoplasm through selective subcellular drug release and hence overcome acquired resistance.

### DISCUSSION

Colorectal cancer is a major cause of morbidity and mortality worldwide (1). Oxaliplatin is currently the standard therapy for colorectal cancer, and acquired resistance to oxaliplatin is a major clinical drawback in the treatment of colorectal cancer [virtually all metastatic colorectal cancer becomes resistant to oxaliplatin, with a median time to progression of 8.7 months (40)]. The major cellular processes by which oxaliplatin enters and attacks cancer cells include uptake and transport, formation of DNA adducts and their recognition by damage response proteins, and signal transduction leading to apoptosis. Any factors that interfere with these pathways can lead to drug resistance (41). Here, we showed

that DACHPt/m can overcome drug resistance by circumventing recognition by MTR and MT1Q, and achieve subcellular drug delivery both *in vitro* and *in vivo* to the perinuclear region of cells. It has been reported that drug delivery systems can overcome multidrug resistance

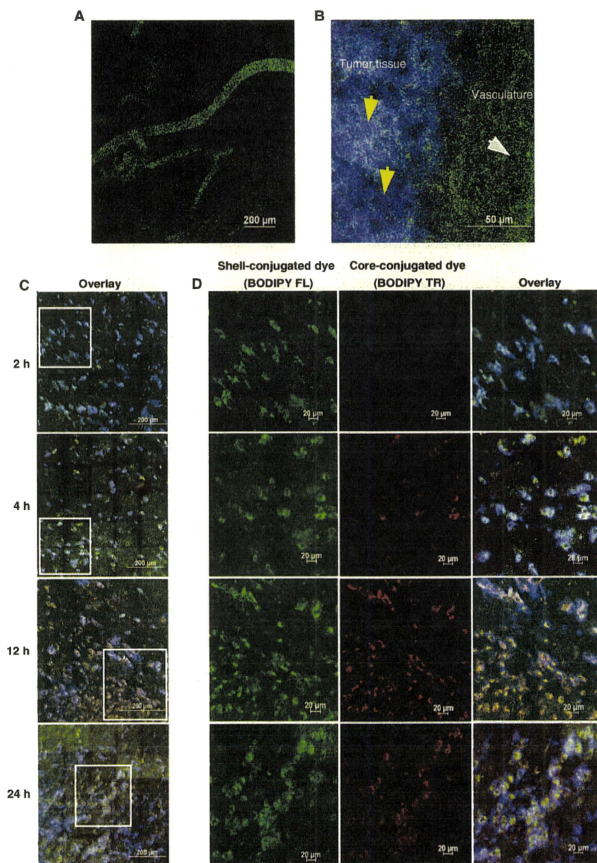


**Fig. 5.** *In vivo* CLSM observation of F-DACHPt/m in blood vessels and tumors after intravenous administration. (A and B) CLSM observation of F-DACHPt/m in the blood vessels of solid tumors (A) immediately after injection and (B) in the tumor tissue at 12 hours after injection. Yellow arrows, tumor tissue; white arrow, blood vessel. (C) Time-dependent CLSM observation of F-DACHPt/m in the tumor tissues at 2, 4, 12, and 24 hours after injection. Green, fluorescence from the shell-conjugated dyes (BODIPY FL); red, core-conjugated dyes (BODIPY TR); blue, cell surfaces stained by CellMask. (D) Magnification of selected areas (square regions in C) by channel.

by avoiding the drug efflux mechanism of P-glycoprotein (20–22). Because P-glycoprotein is not associated with platinum drug resistance (42), we used a different approach. Our data indicate that cytoplasmic detoxification mechanisms against platinum drugs can potentially be avoided by using the appropriate drug delivery system.

Nanocarriers encounter numerous barriers *in vivo en route* to their target during the processes of blood circulation, extravasation, penetration, and cellular uptake. It is therefore difficult to extrapolate *in vivo* outcomes of a drug-nanocarrier combination from its *in vitro* behavior, although real-time observation of *in vivo* behaviors such as we have used here can ascertain critical barriers residing in a living body and facilitate the design of a nanocarrier optimized for *in vivo* delivery. The *in vivo* CLSM technique that we used in this study enabled spatiotemporal and quantitative analyses of extravasation, tissue penetration, and cellular internalization of nanocarriers in living animals. Using dual fluorescent labeling of DACHPt/m, we elucidated the real-time intratumoral behavior of DACHPt/m. The dual fluorescent label of DACHPt micelles allowed us to trace the micelles' position by the ever-present fluorescent signal from the surface of the micelles, and the drug release and dissociation of the multimolecular structure of the micelles by the quenching and fluorescence recovery of the core-conjugated dye. In *in vitro* cellular experiments, these micelles were internalized intact, and then they were disassembled and the drug was released in late endosomes. In our *in vivo* microscopy, we observed that DACHPt/m maintained their micelle form during circulation in the blood, probably because of the stable inner core structure formed by the polymer-metal complexes, and extravasated into solid tumors. DACHPt/m was able to deeply penetrate cancerous tissue after extravasation and was internalized by different cell populations that were distant from the blood vessels. Such efficient penetration of tissue is a requirement of successful drug delivery and a prerequisite for effective subcellular targeting. It has been reported that PEG-modified liposomes with 100-nm diameter accumulated at perivascular regions of solid tumors and failed to penetrate the tumor interstitium deeply (43). Although this characteristic may depend on the cancer type, it is possible that the deep tumor penetration of DACHPt/m is a result of their smaller 30-nm size. Finally, the DACHPt/m structure dissociated at the perinuclear regions of the cell after internalization, based on the pH and chloride ion concentration-selective release of DACHPt. This observation is also consistent with our hypothesis that DACHPt/m can overcome oxaliplatin resistance in tumors by bypassing the cytoplasmic detoxification mechanisms of MTR and MTR1Q. There are, however, several limitations to the type of study that we have performed in a subcutaneous tumor model. Compared with subcutaneous tumors, orthotopic and spontaneously forming tumors may have characteristic differences such as vascular density and degree of fibrosis, which may affect the transport of nanocarriers (44).

Our research provides one approach for subcellular targeting of cytoplasmic drugs. Such nanocarriers have the potential to enhance the drug efficacy and overcome drug resistance.

## MATERIALS AND METHODS

### Materials

$\gamma$ -Benzyl L-glutamate and bis(trichloromethyl) carbonate (triphosgene) were purchased from Sigma Chemical and Tokyo Kasei Kogyo, respec-

tively. *N,N*-Dimethylformamide (DMF), 3-(4,5-dimethylthiazol-2-yl)-2,5-diphenyltetrazolium bromide (MTT), and dimethyl sulfoxide (DMSO) were purchased from Wako Pure Chemicals. Oxaliplatin and NaCH<sub>3</sub>CN were purchased from Sigma-Aldrich Inc. Dichloro(1,2-diamino cyclohexane) platinum(II) was purchased from W. C. Heraeus GmbH.  $\alpha$ -Methoxy- $\omega$ -amino-poly(ethylene glycol) [CH<sub>3</sub>O-PEG-NH<sub>2</sub>; molecular weight (MW), 12,000] was purchased from Nippon Oil and Fats. BODIPY TR-succinimidyl ester, BODIPY FL-hydrazide, LysoTracker Blue, CellLight Early Endosome-RFP (Rab5a-RFP), CellMask, and Lipofectamine RNAiMAX were purchased from Invitrogen.

### Cell lines and animals

HT29 cells were purchased from the American Type Culture Collection. HT29 cells were maintained in McCoy's 5A modified medium (Invitrogen) containing 10% fetal bovine serum (Gibco) as well as 1% penicillin and streptomycin (Sigma) and were cultured at 37°C in a humidified atmosphere of 5% CO<sub>2</sub>. To develop HT29/ox cells (45), we treated HT29 cells with oxaliplatin at IC<sub>50</sub> doses for 1 hour. After 24 hours, cells were subcultured into new flasks and oxaliplatin was added to a culture of 80% confluent cells. The concentration was incrementally increased by factors of 1.2 to 2. The process was continued until the cells were resistant to drug concentrations at least 10 times as great. BALB/c-nu/nu mice (female; body weight, 18 to 20 g; age, 6 weeks old) were purchased from Charles River Japan. All animal experiments were carried out in accordance with the guidelines for animal experiments at the University of Tokyo, Japan.

### Methods

**Synthesis of block copolymers.**  $\alpha$ -(Diethoxymethyl)benzyl- $\omega$ -amino-poly(ethylene glycol) (Ac-Bz-PEG-NH<sub>2</sub>) was previously synthesized in our laboratory (46). Poly(ethylene glycol)-*b*-poly(L-glutamic acid) [PEG-*b*-P(Glu)] [MW<sub>PEG</sub>, 12,000; polymerization degree of P(Glu), 20] and Ac-Bz-PEG-*b*-poly(L-glutamic acid) [Ac-Bz-PEG-*b*-P(Glu)] [MW<sub>PEG</sub>, 12,000; polymerization degree of P(Glu), 20] were synthesized according to the previously described synthetic method (47). Briefly, *N*-carboxyanhydride of  $\gamma$ -benzyl L-glutamate (BLG-NCA) was synthesized by the Fuchs-Farthing method with triphosgene (48). BLG-NCA was polymerized in DMF initiated by the amino group of CH<sub>3</sub>O-PEG-NH<sub>2</sub> or Ac-Bz-PEG-NH<sub>2</sub> to obtain PEG-*b*-poly( $\gamma$ -benzyl L-glutamate) (PEG-*b*-PBLG) or Ac-Bz-PEG-*b*-PBLG, respectively. The MW distribution of PEG-*b*-PBLG and Ac-Bz-PEG-*b*-PBLG was determined by gel permeation chromatography (GPC) [column, TSK-gel G3000HHR, G4000HHR (Tosoh); eluent, DMF containing 10 mM LiCl; flow rate, 0.8 mL/min; detector, refractive index; temperature, 25°C]. PEG-*b*-PBLG and Ac-Bz-PEG-*b*-PBLG showed narrow MW distributions ( $M_w/M_n$ : 1.09 and 1.16, respectively) in GPC. The degrees of polymerization of PBLG in PEG-*b*-PBLG and Ac-Bz-PEG-*b*-PBLG were determined to be 20 by comparing the proton ratios of methylene units in PEG (-OCH<sub>2</sub>CH<sub>2</sub>-;  $\delta$  = 3.7 ppm) and phenyl groups of PBLG (-CH<sub>2</sub>C<sub>6</sub>H<sub>5</sub>;  $\delta$  = 7.3 ppm) in <sup>1</sup>H-NMR (nuclear magnetic resonance) measurement. Both PEG-*b*-PBLG and Ac-Bz-PEG-*b*-PBLG were deprotected by mixing with 0.5 N NaOH at room temperature to obtain PEG-*b*-P(Glu) and Ac-Bz-PEG-*b*-P(Glu), respectively. Complete deprotection was confirmed by <sup>1</sup>H NMR measurement.

**Preparation of micelles.** For conjugation of BODIPY TR to a polymer, a solution of BODIPY TR-succinimidyl ester in DMSO (1 mg/mL) was mixed with Ac-Bz-PEG-*b*-P(Glu). The reaction was carried out overnight at room temperature with stirring. Unreacted

BODIPY TR was removed by dialysis [MW cutoff (MWCO) size, 2000 daltons] against DMSO and water. To conjugate BODIPY FL to the Ac-Bz-PEG-*b*-P(Glu)-BODIPY TR polymer, we mixed a solution of BODIPY FL-hydrazide in DMSO with the polymer, followed by the addition of 1 N HCl to deprotect the acetal group. Samples were stirred overnight at room temperature and treated with NaBH<sub>3</sub>CN to reduce the link between BODIPY FL and the polymer. For purification, unbound BODIPY FL was removed by dialysis (MWCO, 2000 daltons) against DMSO and water. The prepared BODIPY FL-PEG-*b*-P(Glu)-BODIPY TR copolymer was freeze-dried overnight and stored at -20°C. DACHPt/m and F-DACHPt/m were prepared according to the previously described method (23). DACHPt (5 mM) was suspended in distilled water and mixed with silver nitrate ([AgNO<sub>3</sub>]/[DACHPt] = 1) to form aqueous complexes. The solution was kept in the dark at 25°C for 24 hours. AgCl precipitates were eliminated by centrifugation. The supernatant was purified by passage through a 0.22-μm filter. DACHPt aqueous complex solution was then mixed with PEG-*b*-P(Glu) or BODIPY FL-PEG-*b*-P(Glu)-BODIPY TR ([Glu] = 5 mM; [DACHPt]/[Glu] = 1.0) and reacted for 120 hours to obtain DACHPt/m or F-DACHPt/m, respectively. DACHPt/m and F-DACHPt/m were purified by ultrafiltration (MWCO, 30,000 daltons; Fig. 1A). The size distributions of DACHPt/m and F-DACHPt/m were evaluated by dynamic light scattering at 25°C with a Zetasizer Nano ZS90 (Malvern Instruments). The platinum content of DACHPt/m was determined by ion-coupled plasma mass spectrometry (4500 ICP-MS; Hewlett Packard).

**Drug release and fluorescence profiles of micelles under different conditions.** The release of platinum from DACHPt/m and F-DACHPt/m in phosphate-buffered saline (PBS) at 37°C was evaluated as described (23). Briefly, a micelle solution of known platinum concentration was placed inside a dialysis bag (MWCO, 2000 daltons). The solution was then dialyzed against PBS under different conditions mimicking the extracellular environment (10 mM PBS, pH 7.4, and 150 mM NaCl), early endosomes (10 mM PBS, pH 6.9, and 20 mM NaCl), and late endosomes (10 mM PBS, pH 5.5, and 70 mM NaCl) at 37°C (25). The concentration of platinum present in the dialysate was determined with ICP-MS. The fluorescence profiles of F-DACHPt/m were also evaluated under the same conditions with a spectrofluorometer (FP6600, Jasco) or NanoDrop (ND3300, Scrum). Changes in fluorescence intensity were measured at a defined time period.

**In vitro observation of subcellular localization and the fate of F-DACHPt/m by CLSM.** HT29 cells were cultured at  $1 \times 10^6$  cells in 35-mm glass-based dishes (Asahi Techno Glass). After overnight incubation in a fresh medium, the cells were washed twice with PBS. The medium was then replaced by 1 ml of fresh medium containing F-DACHPt/m (100 μM on Pt base). Live-cell CLSM imaging was performed with a Zeiss LSM 510 META nonlinear optics scan head attached to an inverted Axiovert 200 M SP equipped with a 63 × 1.4 numerical aperture Plan Apochromat oil immersion objective (Carl Zeiss). For long-term time-lapse imaging, culture dishes were wrapped with an optically clear foil cover (Carl Zeiss) to avoid evaporation and mounted onto the microscope stage incubator (37°C, 5% CO<sub>2</sub>, 90% relative humidity). Bright-field DIC (differential interference contrast) images and fluorescent sequences were taken every 30 min for 72 hours. BODIPY FL was excited at 488 nm with an Ar laser and fluorescence was detected at 500 to 530 nm, whereas BODIPY TR was excited at 543 nm with a He-Ne laser, and fluorescence was detected at 565 to 615 nm. Laser power was kept low at 0.36 mW for 488 nm and

at 0.018 mW for 543 nm so that photobleaching was negligible. To determine whether DACHPt/m was taken up by endocytosis, we treated HT29 cells with F-DACHPt/m at 37°C or 4°C for 6 hours and then observed by CLSM. For the colocalization studies, we used micelles prepared from BODIPY FL-PEG-*b*-P(Glu) that only emit fluorescence from the shell. HT29 cells, which had been preincubated with CellLight Early Endosome-RFP to express an early endosome marker, Rab5a-RFP, were treated with BODIPY FL-conjugated DACHPt/m, and images were taken at indicated time points after staining with LysoTracker Blue. Rab5a-RFP was excited at 543 nm with a He-Ne laser, and fluorescence was detected at 565 to 615 nm. LysoTracker Blue was excited in multiphoton mode at 710 nm with a Mai Tai tunable broadband laser (Spectra-Physics), and fluorescence was detected at 390 to 465 nm. Colocalization was quantified as follows:

$$\text{amount of colocalization (\%)} \\ = \text{BODIPY FL pixels}_{\text{colocalization}} / \text{BODIPY FL pixels}_{\text{total}} \times 100$$

where BODIPY FL pixels<sub>colocalization</sub> represents the number of BODIPY FL pixels colocalizing with Rab5a-RFP or LysoTracker pixels in the cytoplasm, and BODIPY FL pixels<sub>total</sub> represents the number of all BODIPY FL pixels in the cytoplasm. The timing and location of the micelle dissociation and concomitant drug release were studied by evaluating the colocalization of BODIPY FL and BODIPY TR signals from F-DACHPt/m with the late endosomes/lysosomes (Fig. 3, E and F). Cells were treated with F-DACHPt/m, and images were taken at indicated time points after staining with LysoTracker Blue. Colocalization was quantified as follows:

$$\text{amount of colocalization (\%)} \\ = \text{BODIPY FL or BODIPY TR pixels}_{\text{colocalization}} / \text{BODIPY FL or BODIPY TR pixels}_{\text{total}} \times 100$$

where BODIPY FL or BODIPY TR pixels<sub>colocalization</sub> represents the number of BODIPY FL or BODIPY TR pixels colocalizing with LysoTracker pixels in the cytoplasm, and BODIPY FL or BODIPY TR pixels<sub>total</sub> represents the number of all BODIPY FL or BODIPY TR pixels in the cytoplasm.

**Determination of subcellular Pt accumulation and amount of Pt-DNA adducts.** HT29 cells ( $6 \times 10^6$ ) were seeded in 100-mm tissue culture dishes. After 24 hours, cells were treated with 10 μM oxaliplatin or DACHPt/m on a platinum base. After 6, 8, 12, and 24 hours of drug exposure, the medium was removed and the cells were washed three times with PBS, scraped, and harvested. Samples were freeze-dried overnight, dissolved in heated nitric acid, and evaporated to dryness. The samples were redissolved in water and the Pt content was determined by ICP-MS. For the quantification of Pt-DNA adducts, DNA was extracted with a DNA purification kit (Promega) according to the manufacturer's protocol. The amount and purity of DNA were determined by measuring absorption at 260 and 280 nm with NanoDrop (ND3300). The DNA was dissolved in nitric acid, dried, and redissolved in water. The Pt content was determined by ICP-MS, and the DNA platinum levels were expressed as micrograms of Pt per milligram of DNA.

**In vitro cytotoxicity study against human cancer cells.** The in vitro cytotoxicity of oxaliplatin and DACHPt/m was examined against a panel of 37 human cancer cells as described (34, 35). Cancer cells were plated into flat-bottomed 96-well plates at  $5 \times 10^3$  per well. Cells were treated by continuous exposure to oxaliplatin or DACHPt/m in a final volume of 100 μl. Plates were incubated for 48 hours at 37°C in a humidified atmosphere with 5% CO<sub>2</sub>, and cell viability was determined

by MTT assay. To determine the relationship between cellular sensitivity to oxaliplatin or DACHP1/m and the expression of genes involved in the sensitivity or resistance of cells to platinum compounds, we assessed the gene expression profile of 21 human cancer cell lines for 26 genes selected on the basis of previous studies on cisplatin- or oxaliplatin-resistant cells (36). Expression of these individual genes was determined by searching the National Cancer Institute database. The coefficient of correlation between the  $GI_{50}$ s of free oxaliplatin and DACHP1/m as well as the level of gene expression was calculated for each gene.

**Quantitative real-time RT-PCR.** The expression of the metallo-thionein (MT1Q) [human MT1B (same as MT1Q), NM\_005947, 4MQ-012725-01-0002] and methionine synthase (MTR) (human MTR, NM\_000254, 4LQ-009896-00-0002) was confirmed by quantitative real-time RT-PCR. After 24 hours of treatment, cells were washed with PBS and harvested. Total RNA was prepared with TRIzol (Invitrogen), and complementary DNA (cDNA) was reverse-transcribed with a QuantiTect reverse transcription kit (Qiagen). PCR primer sequences were as follows: MT1Q, 5'-GAATCCAGGCTTGTCTTGG-3' (forward) and 5'-CATTTGGACATCTTGCACCTTG-3' (reverse); MTR, 5'-ACCCAACITCCAGGGAGACT-3' (forward) and 5'-GGCAC-CATGATCTTGGACTT-3' (reverse); actin, 5'-AGATGTGGATCAG-CAGCAG-3' (forward) and 5'-GCGCAAGTTAGGTTTGTGCA-3' (reverse); and 18S, 5'-CGGGCAGACCCATTGGAAC-3' (forward) and 5'-GAATCGAACCCTGATTCGCCGTC-3' (reverse). cDNA from HT29 cells was amplified with specific primers with a SYBR Green Core Reagent Kit (Qiagen) and a real-time PCR instrument (Applied Biosystems). Expression of each gene was standardized with endogenous actin or 18S as a control, and its relative levels in HT29 or HT29/ox cells were quantified by calculating  $2^{-\Delta\Delta C_T}$ , where  $\Delta\Delta C_T$  is the difference in  $C_T$  (cycle number at which the amount of amplified target reaches a fixed threshold) between target and reference.

**MT1Q and MTR gene knockdown.** The siRNAs against MT1Q and MTR and the control siRNA were purchased from Thermo Fisher Scientific Inc. The siRNA target sequences against MT1Q are the following: siMT1Q, GCAAAGGCCUCAUCAGAGAA. The siRNA sequences against MTR are the following: siMTR, CUGAGAAAGCCUUAACGUUA. The siRNAs were transfected into the cell with Lipofectamine RNAiMAX (Invitrogen) according to the instructions of the manufacturer. Briefly, HT29/ox cells ( $4 \times 10^5$ ) were seeded in six-well plates. Twenty-four hours later, the mixture of siMT1Q (50 nM) and siMTR (50 nM) was transfected into the cells with Lipofectamine RNAiMAX reagent. Knockdown of MT1Q and MTR was separately confirmed by real-time PCR (fig. S6, A and B, respectively). To investigate the role of MT1Q and MTR in the oxaliplatin resistance in HT29/ox cells, we seeded HT29/ox cells ( $5 \times 10^5$ ) in 96-well plates, and 24 hours later, the mixture of siMT1Q (50 nM) and siMTR (50 nM) or the control siRNA was transfected into the cells with Lipofectamine RNAiMAX reagent. Twenty-four hours after transfection, the transfected HT29/ox cells were treated by continuous exposure to oxaliplatin in a final volume of 100  $\mu$ l. Plates were further incubated for 48 hours at 37°C in a humidified atmosphere with 5% CO<sub>2</sub>, and their cytotoxicity was determined by MTT assay.

**Western blotting.** HT29 or HT29/ox cells ( $5 \times 10^6$ ) were seeded in 100-mm<sup>2</sup> plates and washed with PBS (100  $\mu$ l). Cell extracts were resolved in TNE buffer [1% NP-40, 150 mM NaCl, 10 mM tris-HCl, 1 mM EDTA, aprotinin (10  $\mu$ g/ml), 2 mM Na<sub>2</sub>VO<sub>4</sub>, 10 mM NaF]. The cell suspension was centrifuged for 20 min at 15,000g. Sampling buffer (4x) was added to the aliquots, followed by incubation

for 5 min at 100°C. Transfer to a polyvinylidene difluoride membrane (Invitrogen) was performed by electrophoresis for 90 min at 125 V. Membranes were blocked with 6% nonfat milk or tris-buffered saline (TBS) with 0.1% Tween 20 (MT1Q) for 1 hour. They were then probed at room temperature with the following antibodies: anti-metallothionein (ab12228, 1:1,000, Abcam), anti-methionine synthase (ab66039, 1:2,000, Abcam), and anti- $\beta$ -actin (#4967, 1:10,000, Cell Signaling). Membranes were washed three times with washing buffer (TBS with 0.1% Tween 20) and then probed with the secondary anti-rabbit immunoglobulin G (IgG) horseradish peroxidase (HRP) (W401B, 1:10,000, Promega) or anti-mouse IgG HRP (W402B, 1:10,000, Promega) conjugate for 1 hour. The secondary antibody was washed three times with washing buffer and then evenly coated with enhanced chemiluminescence (ECL) Western blotting detection reagents (GE Healthcare) for 30 s. The membrane was immediately exposed to Fuji Medical X-ray film (Fujifilm) at room temperature for various periods in a film cassette. Protein levels were standardized with the signal from the  $\beta$ -actin probe.

**In vivo antitumor activity studies.** BALB/c-nu/nu mice (female,  $n = 4$ ) were inoculated subcutaneously with HT29 or HT29/ox cells ( $1 \times 10^7$ /ml). Tumors were allowed to grow for 1 week (tumor size at this point was about 40 mm<sup>3</sup>). Mice were then treated intravenously three times at 2-day intervals with oxaliplatin (8 mg/kg) or DACHP1/m (4 mg/kg) on a platinum base. Antitumor activity was evaluated in terms of tumor size ( $V$ ) with the following equation:

$$V = a \times b^2/2$$

Here,  $a$  and  $b$  are the major and minor axes, respectively, of the tumor as measured by a caliper.

**Intravital observation of the in vivo behavior of F-DACHP1/m.** Intravital observation of F-DACHP1/m was performed as described (49). Female BALB/c mice (6 to 8 weeks old) were inoculated subcutaneously with HT29 cells ( $1 \times 10^7$ /ml). After 5 days, when the tumor volumes reached 70 mm<sup>3</sup>, F-DACHP1/m (10 mg/kg) was administered intravenously. At 2, 4, 12, and 24 hours after treatment, mice were anesthetized with 2.5% isoflurane (Abbott Japan) with a Univentor 400 Anesthesia Unit (Univentor). An arc-shaped incision was made around the subcutaneous tumor, and the skin flap was elevated without injuring the feeding vessels. The mouse was placed directly onto a thermoplate (Tokai Hit), and the skin flap was everted and stretched with several bent 30-gauge needles. The plasma membrane stain, CellMask Deep Red, was directly applied to the subcutaneous tumor, and a coverslip (Muto Pure Chemicals) was attached with just enough pressure to flatten the tumor surface. All in vivo images were acquired with a Nikon A1R CLSM attached to an upright Eclipse FN1 (Nikon). The A1R incorporates a conventional galvano scanner and a high-speed resonant scanner. The latter allows an acquisition speed of 30 frames per second while maintaining a relatively high resolution of 512  $\times$  512 scanned points. BODIPY FL, BODIPY TR, and CellMask were excited with three lasers (488-nm Ar, 560-nm He-Ne, and 640-nm He-Ne lasers), and the fluorescent signals were detected. Laser powers were kept at 19.5 mW for 488-nm Ar, 7.5 mW for 561-nm He-Ne, and 1 mW for 640-nm He-Ne.

**Statistical analysis.** Data are presented as means  $\pm$  SEM. The significant differences between the groups were analyzed by a Student's  $t$  test, and a  $P$  value of <0.05 was considered significant.

## SUPPLEMENTAL MATERIAL

www.sciencetranslationalmedicine.org/cgi/content/full/3/6/64ra2/DC1

Fig. S1. Schematic scheme of BODIPY FL-PEG-b-P(Glu)-BODIPY TR.

Fig. S2. Size distribution of DACHP/m and F-DACHP/m as determined by dynamic light scattering.

Fig. S3. Fluorescent images of H2929 cells after F-DACHP/m at 37°C and 4°C.

Fig. S4. In vitro CLSM observation of dissociation of F-DACHP/m in the late endosomes/lysosomes.

Fig. S5. In vitro cytotoxicity of oxaliplatin and DACHP/m against a human cancer cell panel.

Fig. S6. Knockdown of MTH1 and MTR restores the sensitivity of H2929 to oxaliplatin.

Fig. S7. Schematic illustration of experimental settings of in vivo CLSM.

Table S1. Coefficient of correlation between the  $GI_{50}$  of free oxaliplatin or DACHP/m and the expression levels of genes involved in the sensitivity or resistance of cells to platinum compounds.

Video S1. In vivo live imaging.

Video S2. In vivo live imaging (immediately after injection).

Video S3. In vivo live imaging (12 hours after injection).

## REFERENCES AND NOTES

- Jamal, R. Siegel, E. Ward, Y. Hao, J. Xu, M. J. Thun, Cancer statistics, 2009. *CA Cancer J. Clin.* **59**, 225–249 (2009).
- M. Allen, P. R. Cullis, Drug delivery systems: Entering the mainstream. *Science* **303**, 1818–1822 (2004).
- M. Ferrari, Cancer nanotechnology: Opportunities and challenges. *Nat. Rev. Cancer* **5**, 161–171 (2005).
- V. P. Torchilin, Recent advances with liposomes as pharmaceutical carriers. *Nat. Rev. Drug Discov.* **4**, 145–160 (2005).
- R. Duncan, The dawning era of polymer therapeutics. *Nat. Rev. Drug Discov.* **2**, 347–360 (2003).
- Y. Matsumura, H. Maeda, A new concept for macromolecular therapeutics in cancer chemotherapy: Mechanism of tumorotropic accumulation of proteins and the antitumor agent Smilax. *Cancer Res.* **46**, 6387–6392 (1986).
- M. E. Davis, Z. G. Chen, D. M. Shin, Nanoparticle therapeutics: An emerging treatment modality for cancer. *Nat. Rev. Drug Discov.* **7**, 771–782 (2008).
- N. Nishiyama, K. Kataoka, Current state, achievements, and future prospects of polymeric micelles as nanocarriers for drug and gene delivery. *Pharmacol. Ther.* **112**, 630–648 (2006).
- M. Yokoyama, M. Miyachi, N. Yamada, T. Okano, Y. Sakurai, K. Kataoka, S. Inoue, Characterization and anticancer activity of the micelle-forming polymeric anticancer drug adriamycin-conjugated poly(ethylene glycol)-poly(aspartic acid) block copolymer. *Cancer Res.* **50**, 1693–1700 (1990).
- K. Kataoka, G. S. Kwon, M. Yokoyama, T. Okano, Y. Sakurai, Block copolymer micelles as vehicles for drug delivery. *J. Control. Release* **24**, 119–132 (1993).
- K. Kataoka, A. Harada, Y. Nagasaki, Block copolymer micelles for drug delivery: Design, characterization and biological significance. *Adv. Drug Deliv. Rev.* **47**, 113–131 (2001).
- A. V. Kabanov, E. V. Bratskova, D. W. Miller, Pluronic block copolymers as modulators of drug efflux transporter activity in the blood-brain barrier. *Adv. Drug Deliv. Rev.* **55**, 151–164 (2003).
- Y. Matsumura, K. Kataoka, Preclinical and clinical studies of anticancer agent-incorporating polymeric micelles. *Cancer Sci.* **100**, 572–579 (2009).
- Y. Matsumura, T. Hamaguchi, T. Ura, K. Muro, Y. Yamada, Y. Shimada, K. Shirota, T. Okusaka, H. Ueno, M. Ikeda, N. Watanabe, Phase I clinical trial and pharmacokinetic evaluation of NK911, a micelle-encapsulated doxorubicin. *Br. J. Cancer* **91**, 1775–1781 (2004).
- T. Hamaguchi, K. Kato, H. Yasui, C. Morizane, M. Ikeda, H. Ueno, K. Muro, Y. Yamada, T. Okusaka, K. Shirota, Y. Shimada, H. Nakahama, Y. Matsumura, A phase I and pharmacokinetic study of NK105, a paclitaxel-incorporating micellar nanoparticle formulation. *Br. J. Cancer* **97**, 170–176 (2007).
- T. Hamaguchi, T. Doi, T. Eguchi-Nakajima, K. Kato, Y. Yamada, Y. Shimada, N. Fuse, A. Ohtsu, S. Matsumoto, M. Takanashi, Y. Matsumura, Study I of NK012, a novel SN-38-incorporating micellar nanoparticle, in adult patients with solid tumors. *Clin. Cancer Res.* **16**, 5058–5066 (2010).
- R. H. Wilson, R. Plummer, J. Adam, M. M. Eatock, A. V. Boddy, M. Griffin, R. Miller, Y. Matsumura, T. Shimizu, H. Calvert, Phase I and pharmacokinetic study of NC-6004, a new platinum entity of cisplatin-conjugated polymer forming micelles. *J. Clin. Oncol.* **26**, 2573 (2008).
- R. Dent, M. Trudeau, K. I. Pritchard, W. M. Hanna, H. K. Kahn, C. A. Sawka, L. A. Lickley, E. Rawlinson, P. Sun, S. A. Narod, Triple-negative breast cancer: Clinical features and patterns of recurrence. *Clin. Cancer Res.* **13**, 4429–4434 (2007).
- J. A. Hubbell, Materials science. Enhancing drug function. *Science* **300**, 595–596 (2003).
- T. Minko, P. Kopecková, J. Kopeček, Efficacy of the chemotherapeutic action of HPMA copolymer-bound doxorubicin in a solid tumor model of ovarian carcinoma. *Int. J. Cancer* **86**, 1008–1117 (2000).
- D. Kim, E. S. Lee, K. T. Oh, Z. G. Gao, Y. H. Bae, Doxorubicin-loaded polymeric micelle overcomes multidrug resistance of cancer by double-targeting folate receptor and early endosomal pH. *Small* **4**, 2043–2050 (2008).
- K. Cho, X. Wang, S. Nish, Z. G. Chen, D. M. Shin, Therapeutic nanoparticles for drug delivery in cancer. *Clin. Cancer Res.* **14**, 1310–1316 (2008).
- H. Cabral, N. Nishiyama, S. Okazaki, H. Koyama, K. Kataoka, Preparation and biological properties of dichloro(1,2-diaminocyclohexane)platinum(II) (DACHP/m)-loaded polymeric micelles. *J. Control. Release* **101**, 223–232 (2005).
- H. Cabral, N. Nishiyama, K. Kataoka, Optimization of (1,2-diamino-cyclohexane)platinum(II)-loaded polymeric micelles directed to improved tumor targeting and enhanced antitumor activity. *J. Control. Release* **121**, 146–155 (2007).
- N. D. Sonawane, J. R. Thiagarajah, A. S. Verkman, Chloride concentration in endosomes measured using a ratioable fluorescent Cl<sup>-</sup> indicator: Evidence for chloride accumulation during acidification. *J. Biol. Chem.* **277**, 5506–5513 (2002).
- N. Nishiyama, F. Koizumi, S. Okazaki, Y. Matsumura, K. Nishio, K. Kataoka, Differential gene expression profile between PC-14 cells (treated with free cisplatin and cisplatin-incorporated polymeric micelles). *Bioconjug. Chem.* **14**, 449–457 (2003).
- L. D. Johnson, H. C. Kang, R. P. Haugland, Fluorescent membrane probes incorporating dipyrrometheneboron difluoride fluorophores. *Anal. Biochem.* **198**, 228–237 (1991).
- A. Amold, I. Hennenbelle, P. Canal, R. Bugat, S. Guichard, Cellular determinants of oxaliplatin sensitivity in colon cancer cell lines. *Eur. J. Cancer* **39**, 112–119 (2003).
- L. Kelland, The resurgence of platinum-based cancer chemotherapy. *Nat. Rev. Cancer* **7**, 573–584 (2007).
- E. Raymond, S. Falvre, S. Chaney, J. Woyrnarowski, E. Cvitkovic, Cellular and molecular pharmacology of oxaliplatin. *Mol. Cancer Ther.* **1**, 227–235 (2002).
- F. R. Luo, T. Y. Yen, S. D. Wyrwick, S. G. Chaney, High-performance liquid chromatographic separation of the biotransformation products of oxaliplatin. *J. Chromatogr. B Biomed. Sci. Appl.* **724**, 345–356 (1999).
- F. R. Luo, S. D. Wyrwick, S. G. Chaney, Biotransformations of oxaliplatin in rat blood in vitro. *J. Biochem. Mol. Toxicol.* **13**, 159–169 (1999).
- R. Duncan, Polymer conjugates as anticancer nanomedicines. *Nat. Rev. Cancer* **6**, 688–701 (2006).
- T. Yamori, S. Matsumura, S. Sato, K. Yamazaki, A. Komi, K. Ishizu, I. Mita, H. Edaizumi, Y. Matsuba, K. Takewashi, O. Nakahishi, H. Kohno, Y. Nakajima, H. Komatsu, T. Andoh, T. Tsuruo, Potent antitumor activity of MS-247, a novel DNA minor groove binder, evaluated by *in vitro* and *in vivo* human cancer cell line panel. *Cancer Res.* **59**, 4042–4049 (1999).
- S. Yaguchi, Y. Fukui, I. Koshizumi, H. Yoshimi, T. Matsuno, H. Gouda, S. Hirono, K. Yamazaki, T. Yamori, Antitumor activity of ZSTK474, a new phosphatidylinositol 3-kinase inhibitor. *J. Natl. Cancer Inst.* **98**, 545–556 (2006).
- A. Vekris, D. Meynard, M. C. Haaz, M. Bypass, J. Bonnet, J. Robert, Molecular determinants of the cytotoxicity of platinum compounds: The contribution of *in silico* research. *Cancer Res.* **64**, 356–362 (2004).
- S. L. Kelley, A. Basu, B. A. Teicher, M. P. Hacker, D. H. Hamer, J. S. Lazo, Overexpression of metallothionein confers resistance to anticancer drugs. *Science* **241**, 1813–1815 (1988).
- T. Hoffpr, P. J. Beale, F. E. Boxall, S. Y. Sharp, L. R. Kelland, Mechanisms of drug resistance to the platinum complex ZD0473 in ovarian cancer cell lines. *Eur. J. Cancer* **36**, 1984–1990 (2000).
- P. M. Deegan, L. S. Pratt, M. P. Ryan, The neurotoxicity, cytotoxicity and renal handling of a cisplatin-methionine complex in male Wistar rats. *Toxicology* **89**, 1–14 (1994).
- R. M. Goldberg, D. J. Sargent, R. F. Morton, C. S. Fuchs, R. K. Ramaniathan, S. K. Williamson, B. P. Findlay, H. C. Pittot, S. R. Alberts, A randomized controlled trial of fluorouracil plus leucovorin, irinotecan, and oxaliplatin combinations in patients with previously untreated metastatic colorectal cancer. *J. Clin. Oncol.* **22**, 23–30 (2004).
- D. Wang, S. J. Lippard, Cellular processing of platinum anticancer drugs. *Nat. Rev. Drug Discov.* **4**, 307–320 (2005).
- P. Pastan, M. M. Gottesman, K. Ueda, E. Lovelace, A. V. Rutherford, M. C. Willingham, A retrovirus carrying an *MDR1* cDNA confers multidrug resistance and polarized expression of P-glycoprotein in MDCK cells. *Proc. Natl. Acad. Sci. USA* **85**, 4486–4490 (1988).
- R. K. Jain, Delivery of molecular and cellular medicine to solid tumors. *Adv. Drug Deliv. Rev.* **46**, 149–168 (2001).
- Y. Saito, M. Yasunaga, J. Kuroda, Y. Koga, Y. Matsumura, Antitumor activity of NK012, SN-38-incorporating polymeric micelles, in hypovascular orthotopic pancreatic tumor. *Eur. J. Cancer* **46**, 658–658 (2010).
- M. Mishima, G. Samimi, A. Kondo, X. Lin, S. B. Howell, The cellular pharmacology of oxaliplatin resistance. *Eur. J. Cancer* **38**, 1405–1412 (2002).

46. Y. Akiyama, Y. Nagasaki, K. Kataoka, Synthesis of heterotelechelic poly(ethylene glycol) derivatives having  $\alpha$ -benzaldehyde and  $\omega$ -pyridyl disulfide groups by ring opening polymerization of ethylene oxide using 4-(diethoxymethyl)benzyl alkoxide as a novel initiator. *Bioconjug. Chem.* **15**, 424–427 (2004).
47. N. Nishiyama, S. Okazaki, H. Cabral, M. Miyamoto, Y. Kato, Y. Sugiyama, K. Nishio, Y. Matsumura, K. Kataoka, Novel cisplatin-incorporated polymeric micelles can eradicate solid tumors in mice. *Cancer Res.* **63**, 8977–8983 (2003).
48. W. H. Daly, D. Poche, The preparation of N-carboxyanhydrides of  $\alpha$ -amino acids using bis(trichloromethyl)carbonate. *Tetrahedron Lett.* **29**, 5859–5862 (1988).
49. Y. Matsumoto, T. Nomoto, H. Cabral, Y. Matsumoto, S. Watanabe, R. J. Christie, K. Miyata, M. Oba, T. Ogura, Y. Yamasaki, N. Nishiyama, T. Yamasoba, K. Kataoka, Direct and instantaneous observation of intravenously injected substances using intravital confocal micro-videography. *Biomed. Opt. Express* **1**, 1209–1216 (2010).
50. **Acknowledgments:** M.M. thanks J. Ghaugas for his support and suggestions for preparing the manuscript and S. Hiro for his help with in silico data analysis. **Funding:** This research was supported in part by Funding Program for World-Leading Innovative R&D on Science and Technology (FIRST Program) from the Japan Society for the Promotion of Science

(JSPS) and the Core Research Program for Evolutional Science and Technology (CREST) from the Japan Science and Technology Agency (JST). **Author contributions:** M.M. and H.C. designed and performed the experiments, analyzed the results, and wrote the manuscript. Y.M. performed the imaging experiments. S.W. performed the siRNA knockdown studies. T.Y. conducted human cell panel analysis. M.R.K. edited the manuscript. N.N. supervised the project and wrote the manuscript. K.K. supervised the project and edited the manuscript. **Competing interests:** The authors declare that they have no competing interests.

Submitted 14 June 2010

Accepted 10 December 2010

Published 5 January 2011

10.1126/scitranslmed.3001385

**Citation:** M. Murakami, H. Cabral, Y. Matsumoto, S. Wu, M. R. Kano, T. Yamori, N. Nishiyama, K. Kataoka, Improving drug potency and efficacy by nanocarrier-mediated subcellular targeting. *Sci. Transl. Med.* **3**, 64ra2 (2011).



## Antiangiogenic gene therapy of experimental pancreatic tumor by sFlt-1 plasmid DNA carried by RGD-modified crosslinked polyplex micelles

Yelena Vachutinsky<sup>a</sup>, Makoto Oba<sup>b</sup>, Kanjiro Miyata<sup>c</sup>, Shigehiro Hiki<sup>d</sup>, Mitsunobu R. Kano<sup>e</sup>, Nobuhiko Nishiyama<sup>c,f</sup>, Hiroyuki Koyama<sup>b</sup>, Kohei Miyazono<sup>e,f</sup>, Kazunori Kataoka<sup>a,c,d,f,\*</sup>

<sup>a</sup> Department of Bioengineering, Graduate School of Engineering, The University of Tokyo, 7-3-1 Hongo, Bunkyo-ku, Tokyo 113-8656, Japan

<sup>b</sup> Department of Clinical Vascular Regeneration, Graduate School of Medicine, The University of Tokyo, 7-3-1 Hongo, Bunkyo-ku, Tokyo 113-8655, Japan

<sup>c</sup> Center for Disease Biology and Integrative Medicine, Graduate School of Medicine, The University of Tokyo, 7-3-1 Hongo, Bunkyo-ku, Tokyo 113-0033, Japan

<sup>d</sup> Department of Materials Engineering, Graduate School of Engineering, The University of Tokyo, 7-3-1 Hongo, Bunkyo-ku, Tokyo 113-8656, Japan

<sup>e</sup> Department of Molecular Pathology, Graduate School of Medicine, The University of Tokyo, 7-3-1 Hongo, Bunkyo-ku, Tokyo 113-8655, Japan

<sup>f</sup> Center for Nano-Bio Integration The University of Tokyo, 7-3-1 Hongo, Bunkyo-ku, Tokyo 113-8656, Japan

### ARTICLE INFO

#### Article history:

Received 5 October 2009

Accepted 1 February 2010

Available online 6 February 2010

#### Keywords:

Poly(ethylene glycol)-block-poly(L-lysine)

(PEG-PLys)

Cyclic RGD peptide

sFlt-1

Antiangiogenic gene therapy

Polyplex micelle

### ABSTRACT

Disulfide crosslinked polyplex micelles with RGD peptides were formed through ion complexation of thiolated c(RGDK)-poly(ethylene glycol)-block-poly(L-lysine) (c(RGDK)-PEG-P(Lys-SH)) and plasmid DNA encoding sFlt-1 and tested for their therapeutic effect in BxPC3 pancreatic adenocarcinoma tumor bearing mice. These micelles, systemically injected, demonstrated significant inhibition of tumor growth up to day 18, as a result of the antiangiogenic effect that was confirmed by vascular density measurements. Significant therapeutic activity of the 15% crosslinked micelle (c(RGDK)-PEG-P(Lys-SH)15) was achieved by combined effect of increased tumor accumulation, interaction with endothelial cells and enhanced intracellular uptake through receptor-mediated endocytosis. These results suggest that RGD targeted crosslinked polyplex micelles can be effective plasmid DNA carriers for antiangiogenic gene therapy.

© 2010 Elsevier B.V. All rights reserved.

### 1. Introduction

Poly(ethylene glycol) (PEG)-polycation block copolymers have been widely investigated in the field of gene delivery as a potential non-viral vectors for systemic applications [1–7]. The complexes of plasmid DNA (pDNA) and block copolymers form self-assembling particles, termed polyplex micelles, with a core-shell structure. The outer hydrophilic shell layer, formed by PEG segment, increases micelle stability in serum, improves its pharmacokinetic properties, and reduces polymer toxicity [8–11]. Nevertheless, further stabilization and increased longevity in blood are required for polyplex micelles to achieve successful gene delivery *in vivo*.

Disulfide crosslinks were previously introduced into the polyplex micelle core to stabilize its structure in the extracellular entity, while facilitating smooth release of the entrapped pDNA in the intracellular reductive environment [12,13]. Indeed, disulfide crosslinked polyplex micelles exhibited improved transfection of the reporter gene to cultured cells and mouse liver upon systemic administration [13]. In addition, cyclic RGD peptide ligands (c(RGDK)) were recently installed

onto the surface of the disulfide crosslinked polyplex micelles to achieve specific targeting to tumor neo-vasculature [14,15]. RGD (Arg-Gly-Asp) peptide is a recognition motif in multiple ligands of  $\alpha_v$  integrin family [16]. Moreover, cyclic RGD peptides showed increased affinity to  $\alpha_v\beta_3$  and  $\alpha_v\beta_5$  integrin receptors [17] which are overexpressed on tumor angiogenic endothelial cells [18]. Therefore, RGD peptide ligands have been intensively investigated as an active targeting strategy in antiangiogenic gene therapy for cancer [19–22]. Consequently, we hypothesized that polyplex micelles with cyclic RGD ligands and disulfide crosslinks may be a useful system for targeting angiogenic endothelial cells by systemic administration. RGD conjugated polyplex micelles showed remarkably increased transfection efficiency in cultured HeLa cells possessing  $\alpha_v\beta_3$  and  $\alpha_v\beta_5$  integrins, as a result of increased cellular uptake and intracellular trafficking of micelles toward perinuclear region via caveolae-mediated endocytosis as was previously reported [14,15]. Caveolae-mediated endocytosis is a nondegradative internalization pathway, which does not result in pH decrease, thus avoiding pDNA degradation in acidic organelles in cell. This route might be especially essential for polylysine based pDNA carriers, which do not possess "proton buffering" ability to escape endosome.

Vascular endothelial growth factor (VEGF) is a major proangiogenic molecule, which stimulates angiogenesis via promoting endothelial proliferation, survival and migration [reviewed in [23,24]]. VEGF and VEGF receptors have been found to be up-regulated in

\* Corresponding author. Department of Bioengineering, Graduate School of Engineering, The University of Tokyo, 7-3-1 Hongo, Bunkyo-ku, Tokyo 113-8656, Japan. Tel: +81 3 5841 7138; fax: +81 3 5841 7139.

E-mail address: kataoka@bme.t.u.tokyo.ac.jp (K. Kataoka).



various types of tumors and are usually associated with tumor progression and poor prognosis (reviewed in [25]). Inhibition of VEGF or its signaling pathway has been shown to suppress tumor angiogenesis and tumor growth [reviewed in [25–27]].

The soluble form of VEGF receptor-1 (soluble fms-like tyrosine kinase-1: sFlt-1) is a potent endogenous agent for antiangiogenic therapy. The sFlt-1 binds to VEGF with the same affinity and equivalent specificity as that of the original receptor, however inhibits its signal transduction [28–30]. Therefore, exogenous sFlt-1 is considered to be an effective therapeutic agent for antiangiogenic tumor therapy [20,21,31–35]. Recently, several reports were published on *in vivo* non-viral gene therapy with sFlt-1, carried by several types of polymers, for inhibition of tumor angiogenesis [21,35]. Kim WJ et al. reported effective tumor growth suppression in CT-26 colon adenocarcinoma bearing mice by systemic injection of polyethyleneimine based polyplexes, utilizing the RGD targeting approach [21].

In this study, thiolated PEG-poly(L-lysine) (PEG-PLys) block copolymer, combining long PEG chain with optimized crosslinking degree, was designed for construction of RGD-mediated gene delivery system. Here we report the therapeutic effect of sFlt-1 expressing pDNA complexed with 15% thiolated control poly(ethylene glycol)-*block*-poly(L-lysine) (PEG-P(Lys-SH15)) and cyclic RGD conjugated (c(RGDK)-PEG-P(Lys-SH15)) polymers, forming crosslinked polyplex micelles, after systemic administration to BxPC3 human pancreas adenocarcinoma tumor bearing mice. Note that BxPC3 xenografts are characterized by heterogeneous vascularity and stroma-rich histology [36], which limits access of therapeutic agents to tumor cells. Thus, the accessibility of endothelial cells by bloodstream, makes antiangiogenic approach an attractive strategy against pancreatic tumor.

## 2. Materials and methods

### 2.1. Materials

*N*-Succinimidyl 3-(2-pyridylidithio)-propionate (SPDP) was purchased from Dojindo Laboratories (Kumamoto, Japan). Cyclo[RGDFK(CX-)] (c(RGDK)) peptides (X = 6-aminocaproic acid; *ε*-AcP) was purchased from Peptide Institute (Osaka, Japan). The PEG-PLys block copolymer (PEG, 17,000 g/mol; polymerization degree of Plys segment, 73) was synthesized as previously reported [37]. Plasmid DNA coding for luciferase (Luc) under the control of CAG promoter was provided by RIKEN Gene Bank (Tsukuba, Japan), and a fragment cDNA of sFlt-1 was inserted into the pCAC vector having CAG promoter. The pDNAs were amplified in competent DH5 $\alpha$  *Escherichia coli* and purified by the HiSpeed Plasmid Maxi Kit purchased from QIAGEN Sciences Co., Inc. (Germantown, MD). Luc pDNA was labeled with Cy5 by the Label IT Nucleic Acid Labeling Kit (Mirus, Madison, WI) according to the manufacturer's protocol. Dulbecco's modified eagle's medium (DMEM) and fetal bovine serum (FBS) were obtained from Sigma-Aldrich Co (Madison, WI) and Dainippon Sumitomo Pharma Co., Ltd. (Osaka, Japan), respectively. Rat monoclonal antibody to CD31 (platelet endothelial cell adhesion molecule 1 (PECAM1)) was purchased from BD Pharmingen (Franklin Lakes, NJ), and Alexa Fluor 488-conjugated secondary antibody to rat IgG was from Invitrogen Molecular Probes (Eugene, OR).

### 2.2. Preparation of block copolymers

#### 2.2.1. Synthesis of thiolated PEG-PLys (PEG-P(Lys-SH))

Pyridylidithiopropionyl (PDP) groups were introduced to the  $\epsilon$ -amino groups of Plys side chain as reported previously [12]. Briefly, acetal-PEG-PLys (83 mg, 2.86  $\mu$ mol) was dissolved in 10 mL *N*-methyl-2-pyrrolidone containing 5wt% LiCl and stirred with a heterobifunctional reagent, SPDP, (10 mg, 31  $\mu$ mol) in the presence of *N,N*-diisopropylethylamine (10 mol excess against the SPDP reagent) for 3 h at room temperature. The mixture was then

precipitated into 20 times excess volume of diethyl ether. The precipitated polymer was dissolved in 10 mM phosphate buffer (pH 7.0, 150 mM NaCl), dialyzed against the same buffer and then distilled water, and lyophilized to obtain PEG-P(Lys-PDP). The degree of PDP substitution for each polymer was determined from the peak intensity ratio of the methylene protons of PEG (OCH<sub>2</sub>CH<sub>2</sub>,  $\delta$  = 3.5 ppm) to the pyridyl protons of the 3-(2-pyridylidithio)propionyl group (C<sub>5</sub>H<sub>4</sub>N,  $\delta$  = 7.2–8.3 ppm) in the <sup>1</sup>H NMR spectrum (D<sub>2</sub>O, 25 °C). Block copolymer with X% thiolation degree was abbreviated as B-SHX%.

#### 2.2.2. Synthesis of c(RGDK)-PEG-P(Lys-SH)

Acetal-PEG-P(Lys-PDP) (30 mg, 1  $\mu$ mol) was dissolved in 10 mM Tris-HCl buffer solution (pH 7.4) (3 mL) with 10 eq. of dithiothreitol (DTT). After 30 min incubation at room temperature, the polymer solution was dialyzed against 0.2 M AcOH buffer (pH 4.0). c(RGDK(CX-)) (8 mg, 6.5 mmol) in AcOH buffer (3 mL) was then added to the polymer solution. After stirring for 5 days, DTT (6.67 mg, 43.9  $\mu$ mol) was added and stirred at room temperature for 3 h. The reacted polymer was purified by dialysis sequentially against 10 mM phosphate buffer pH 7.0 with 150 mM NaCl and distilled water, and lyophilized to obtain c(RGDK)-PEG-P(Lys-SH) [14].

### 2.3. Preparation of polyplex micelles

The above polymers were dissolved in 10 mM Tris-HCl buffer (pH 7.4) containing 10% volume of 100 mM DTT. After 30 min at ambient temperature, twice-excess volume of pDNA solution (50  $\mu$ g/mL) in the same buffer was added to the polymer solution to form a polyplex micelle at *N/P* ratio of 2. The *N/P* ratio was defined as the residual molar ratio of amino groups of thiolated PEG-PLys to phosphate groups of pDNA. After an overnight incubation at ambient temperature, the polyplex micelle solutions were dialyzed against 10 mM Tris-HCl (pH 7.4) containing 0.5% dimethylsulfoxide (DMSO) at 37 °C for 24 h, followed by additional 2 days dialysis for the DMSO removal. During these dialysis processes, thiol groups of the polymers in the micelles were oxidized to form disulfide crosslinks. The concentration of pDNA in each micelle solution was determined by absorbance at 260 nm. Polyplex micelles with and without cyclic RGD peptide ligands were abbreviated as RGD(+) and RGD(-), respectively.

### 2.4. Quantitative determination of transfection efficiency by real time reverse transcription-polymerase chain reaction (RT-PCR) for sFlt-1

HeLa cells, expressing the  $\alpha_v\beta_3$  and  $\alpha_v\beta_5$  integrin receptors, were seeded on 24-well culture plates (10000 cells/well) and incubated for 24 h in 500  $\mu$ L of DMEM medium containing 10% FBS. Micelle solutions were then added at a concentration equivalent to 1  $\mu$ g of pDNA per well and the cells were incubated for 48 h. Following this incubation period, total RNA was extracted from the cells and transcribed to cDNA. The cDNA samples were subjected to polymerase chain reaction (PCR) amplification using the following human specific primers: 5'-CCTACTCCCTTGAACACGAG-3' and 3'-CGCCTTACGGAAGCTCTCT-5'. Amplification conditions were as recommended by the manufacturer (QIAGEN Sciences Co., Inc.). Unknown and standard samples were run in triplicate. Concentrations of unknown samples were interpolated from a standard curve, established by simultaneous amplification of sFlt-1 plasmid standards.

### 2.5. *In vivo* studies

#### 2.5.1. Mice

Five-week-old female Balb/c nude mice were purchased from Charles River Laboratories (Tokyo, Japan). Mice were maintained on ad libitum rodent feed and water. The experimental animals were allowed to acclimate for at least 1 week before tumor implantation. All studies were performed in accordance to the Guide for the Care

and Use of Laboratory Animals as stated by the National Institutes of Health.

### 2.5.2. Tumor implantation

BxPC3 cell line (ATCC, Manassas, VA), derived from human pancreatic tumor was inoculated to nude mice subcutaneously to develop xenografts (100  $\mu$ l of  $5 \times 10^7$  cells/mL PBS suspension). Tumors were allowed to grow for 3 weeks till their size reached approximately 120–160 mm<sup>3</sup>.

### 2.5.3. Blood circulation

Polyplex micelles loading Cy5-labeled pDNA (100  $\mu$ g pDNA/mL, 200  $\mu$ l) were intravenously injected to the mice via the tail vein at a dose of 20  $\mu$ g pDNA/mouse. Blood was collected from the postcaval vein under anesthesia 15 min after injection and centrifuged to obtain blood plasma. Two microliters of 10X trypsin-EDTA were added to 20  $\mu$ l of the plasma and incubated overnight at 37 °C to release pDNA from the micelle by digesting Plys segment of the block copolymer. The fluorescence intensity of the sample solution was measured at  $\lambda = 670$  nm by spectrofluorometer (ND-3300, Nano Drop, Wilmington, DE), and percent of pDNA dosage in the blood was calculated according to the following equation:

$$\% \text{ injected pDNA in the blood} = (F_{670(\text{sample})} / F_{670(\text{control})}) \times 100 \quad (1)$$

where the  $F_{670(\text{control})}$  represents the fluorescence intensity of micelle solution mixed with blood sample (time 0).

### 2.5.4. In vivo tumor growth inhibition

Polyplex micelles, loading pDNA equivalent to 20  $\mu$ g and dissolved in 10 mM Hepes buffer (pH 7.4) with 150 mM NaCl, were administered intravenously on days 0, 4, and 8. Tumor size was measured every 2 days by a digital vernier caliper across its longest (a) and shortest diameters (b) and its volume (V) was calculated according to the formula  $V = 0.5ab^2$ . Tumor progression was evaluated in terms of relative tumor volume (to day 0) over a period of 18 days.

### 2.5.5. Quantification of microvessel density

At the end of *in vivo* tumor growth studies, xenografted tumors were excised and frozen in tissue-Tek-OCT. The frozen tumors were cut into 10  $\mu$ m thick slices with a cryostat maintained at  $-23$  °C. Vascular endothelial cells were immunostained by incubation of the cryosections with anti-CD31 antibody followed by incubation with Alexa Fluor 488-conjugated secondary antibody. The tumor cryosections were observed by a confocal laser scanning microscope (CLSM), LSM 510 (Carl Zeiss, Oberkochen, Germany). Microvessel density was quantified by counting the percentage area of CD31 positive pixels per image with at least 21 images per sample (i.e., three animals per sample  $\times$  7 cryosections per tumor).

### 2.5.6. Micelle accumulation in tumor tissue

Polyplex micelles loading Cy5-labeled pDNA were intravenously injected at a dose of 20  $\mu$ g pDNA/mouse. Mice were sacrificed after 24 h and the excised tumors were fixed in formalin for 1 h, followed by 1 h incubation periods with 10, 15 and 20% sucrose/PBS solutions at room temperature. The tumors were frozen in tissue-Tek-OCT and cryosections were prepared for CLSM visualizations as described in the previous section. The nuclei were stained with Hoechst 33342 (Dojindo Lab, Kumamoto, Japan). The CLSM observations were performed at the excitation wavelengths of 488 nm (Ar laser) for the Alexa Fluor 488, 633 nm (He-Ne laser) for Cy5, and 710 nm (MaiTai laser, two photon excitation) for Hoechst 33342, respectively. The percentage of pDNA positive pixels per image was counted to quantify the micelle accumulation inside the tumor tissue.

### 2.6. Data analysis

The experimental data was analyzed by Student's *t*-test.  $P < 0.05$  was considered as significant.

## 3. Results

Thiolated acetal-PEG-Plys block copolymers, composed of 17 kDa M.W. PEG and 73 lysine units, were prepared as described elsewhere [12,14,37]. SPDP was used as a thiolating reagent and conjugated to the  $\epsilon$ -amino group of lysine unit. Conjugation of c(RGDfK) peptide ligands into the PEG terminus of acetal-PEG-P(Lys-PDP) was achieved through the formation of a thiazolidine ring between the *N*-terminal cysteine and the aldehyde group converted from the acetal group [14,15]. The targetable polyplex micelles were prepared through ion complexation of the above polymers with pDNA at  $N/P = 2$  (Fig. 1), and analyzed for their size and  $\zeta$ -potential by DLS and laser-doppler electrophoresis, respectively. The cumulated diameters of the B-SHX micelles were approximately 104  $\pm$  18 nm, with a moderate polydispersity index of 0.2. The  $\zeta$ -potentials were found to be approximately 0.5 mV, as a result of the PEG palisade formation surrounding the polyplex core [8,14].

Following *in vitro* transfection in HeLa cells, the mRNA expressions of sFlt-1 were quantitatively analyzed by real time RT-PCR. From this analysis, presented in Fig. 2, it is clear that the cells were successfully transfected by the polyplex micelles. The highest transfection efficiency was achieved by RGD(+) B-SH15% crosslinked (15(+)) micelle. Worth noting, detectable protein level of sFlt-1 by ELISA, specific to human VEGF-R1/sFlt-1 (R&D Systems), could be achieved for this formulation only ( $1.2 \pm 0.05$  ng/mL) (data not shown). Other micelles, probably, resulted in sFlt-1 levels which are beyond the sensitivity of this assay ( $< 13$  pg/ml). The increased transfection efficiency of the 15(+) micelle results from the combination of crosslinked core and receptor targeting ligand, consistent with our previous studies [15].

The blood circulation experiments were carried out in BxPC3 tumor bearing mice upon intravenous injections of the Cy5-labeled pDNA (20  $\mu$ g pDNA/ mouse). Blood was collected from the postcaval vein 15 min after administration and analyzed for its fluorescence intensity. Disulfide crosslinks prolonged blood circulation time, while the RGD conjugation resulted in significantly lower blood circulation period of polyplex micelles, as shown in Fig. 3. In the case of crosslinked system, 28% and 21% of injected pDNA were observed in plasma for RGD(–) and RGD(+) micelles, respectively. Significantly lower recovered doses of pDNA, 11% and 7% for RGD(–) and RGD(+) micelles, respectively, were found for non crosslinked system. We further evaluated micelle accumulation in tumor by *in vivo* administration of RGD-conjugated or non-conjugated 15% crosslinked micelles prepared with Cy5-labeled pDNA at a dose of 20  $\mu$ g pDNA/mouse. Both micelles were found to be localized in the tumor blood vessels, 24 h after administration, as was indicated by colocalization of the Cy5-labeled pDNA (red) and the CD31 positive endothelial cells (green) (Fig. 4A). However, quantitative analysis of the pDNA positive area per image revealed significantly higher accumulation of the RGD-conjugated micelle than non-conjugated micelle inside the tumor tissue (Fig. 4B): 3.08% and 2.44% of red pixels per image for RGD(+) and RGD(–) micelle, respectively ( $P < 0.05$ ).

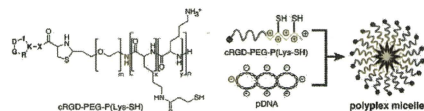
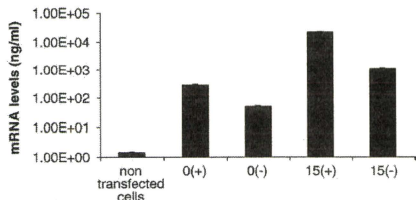


Fig. 1. Structure of cRGD-PEG-P(Lys-SH) and its polyplex micelle.



**Fig. 2.** *In vitro* transfection efficiency of sFlt-1 plasmid DNA in HeLa cells. The cells were transfected with RGD(+) and RGD(-) non crosslinked micelles (0(+)) and 0(-)) and RGD(+) and RGD(-) 15% crosslinked micelles (15(+)) and 15(-)), respectively. Non transfected cells were used as control. Each well was transfected with 1  $\mu$ g of pDNA for 48 h and analyzed for sFlt-1 mRNA levels by real time RT-PCR.

The therapeutic effect of polyplex micelles following intravenous administration of the sFlt-1 expressing pDNA was evaluated by tumor growth inhibition study in BxPC3 tumor bearing mice. When tumors reached the volume of 120–160 mm<sup>3</sup>, animals were injected with three doses of polyplex micelles containing either sFlt-1 or Luc expressing plasmid (20  $\mu$ g pDNA/dose) on days 0, 4 and 8. The results of these studies, in terms of relative tumor volumes (Fig. 5), indicate the ability of RGD(+) and RGD(-) crosslinked polyplex micelles as vehicles for therapeutic gene delivery in BxPC3 tumor bearing mice. In the case of animals treated with 15(+) micelles, the tumor progression was significantly inhibited from day 6, compared to control mice. By the end of the experiment, the mean tumor volume in this group was  $1.67 \pm 0.18$  of initial tumor volume. In the group of animals treated with pDNA encapsulated in RGD(-) micelles, significant inhibition of tumor progression was observed only from day 12, and the mean tumor volume reached  $1.93 \pm 0.52$  of initial tumor volume by the end of the experiment. On the other hand, tumors grew much faster in the control groups, and reached  $2.58 \pm 0.5$  of initial tumor volume.

Intravenous administration of crosslinked polyplex micelles containing sFlt-1 pDNA to BxPC3 tumor bearing mice resulted in significant reduction in the tumor neo-vasculature, as shown by CD31 immunostaining of the tumor cryosections. Representative images are shown in Fig. 6A. Increased density of blood vessels throughout the tissue was observed in control tumors. In contrast, very few blood vessels could be observed in the sFlt-1 treated groups. The quantitative results of microvessel density in tumor tissue cryosections were obtained by counting the area of stained blood vessels (green pixels) per image (Fig. 6B). Systemic administration of sFlt-1 expressing pDNA in the RGD(+) micelles resulted in the lowest average microvessel density of only 8.6% per image, whereas the RGD(-) micelle carrying pDNA led to 12.3% vessels per image. The control group had an average microvessel area of 23.7% per image, significantly higher as compared to the treated groups.

#### 4. Discussion

In this study, we demonstrate that crosslinked polyplex micelles formed by electrostatic interaction of thiolated PEG-Plys block copolymers, modified on their surface with cRGD peptide ligand, and sFlt-1 pDNA are effective for *in vivo* tumor regression upon systemic administration. The thiolated PEG-Plys block copolymer, in this study, was further optimized by higher molecular weight PEG (17,000 Da) against 12,000 Da M.W. PEG used so far [2,3,8,12–15], to achieve enhanced shielding effect and thus higher stability in blood. Block copolymer with 15% thiolation degree, which showed the highest transfection efficiency *in vitro* and *in vivo* (data not shown), was selected for construction of RGD-mediated gene delivery vector.

The results of sFlt-1 transfection in HeLa cells show higher mRNA expression levels in the cells transfected by RGD(+) crosslinked micelle relative to either RGD(-) or non crosslinked micelles (Fig. 2). This result is consistent with our previous studies, indicating the greater stability of crosslinked micelles in the medium and specific affinity of RGD ligand to  $\alpha_v\beta_3$  and  $\alpha_v\beta_5$  integrin receptors expressed in HeLa cells [14,15]. Micelle internalization to the cell via integrin-mediated endocytosis contributes to the accelerated accumulation of pDNA in the perinuclear region through the change in its intracellular trafficking from clathrin-mediated to caveolae-mediated endocytosis, resulting in enhancement of gene expression [15].

When administered intravenously into BxPC3 tumor bearing mice, blood levels of Cy5-labeled pDNA were significantly lower for the RGD(+) micelle compared to the RGD(-) micelle. This observation might be partly explained by enhanced accumulation of pDNA in tumor site when carried by RGD(+) micelle over RGD(-) (Fig. 4B) and other organs as well. These observations are in good agreement with other works using cyclic RGD-modified particles, which reported significantly lower blood circulation times [38–40] while higher accumulation in tumor tissue [21,38–41], liver [21,38–42] and spleen [28–31] compared to the control. Moreover, CLSM observations demonstrated colocalization of both micelles with tumor endothelial cells, confirming their potential as effective antiangiogenic gene delivery vehicles (Fig. 4A).

*In vivo* tumor growth assay revealed significant ( $P < 0.05$ ) tumor growth inhibition when the sFlt-1 pDNA was administered by crosslinked micelles as compared to control groups. Compared to RGD(-), the RGD(+) micelle was more effective in suppressing tumor growth. The significant difference in relative tumor volumes between RGD(+) injected and control groups was observed from day 6 till the end of the experiment. In comparison, significant difference between RGD(-) injected and control groups was observed only from day 12. In addition, relative tumor volumes in the RGD(+) injected group were lower than those in the RGD(-). These findings may be explained by greater tumor accumulation and higher transfection efficiency of RGD-modified micelle, resulted from more effective intracellular plasmid delivery through specific receptor binding and endocytosis. The lack of significant difference in relative tumor volumes between the RGD(+) and RGD(-) injected groups might be due to the lower circulation time in blood of the RGD(+) micelle and its enhanced accumulation in organs such as liver and spleen. Accumulation in liver [21,38–42] and spleen [39–42] was shown for various cyclic RGD-modified vectors and was, in general, attributed to their accelerated clearance through the phagocytosis by macrophages located on reticuloendothelial system (RES) [39–41].

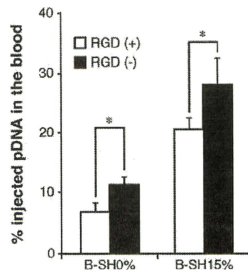


**Fig. 3.** Blood circulation of plasmid DNA carried by RGD (+/–) polyplex micelles. Micelles loading Cy5-labeled pDNA were intravenously administered to the tumor bearing mice (20  $\mu$ g pDNA/mouse). Blood was collected 15 min after administration and analyzed for its fluorescence intensity.  $N = 3$ , Mean  $\pm$  s.d. \* $P < 0.05$  compared to RGD(-).

The antiangiogenic effect of expressed sFlt-1 was confirmed by CD31 immunostaining of the tumor cryosections and quantification of microvessel density. From these studies, it is clear that sFlt-1 was able to significantly suppress tumor neo-vasculature formation when the

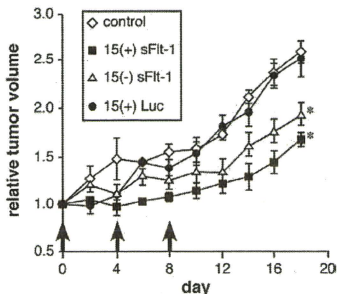
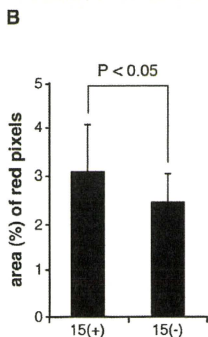
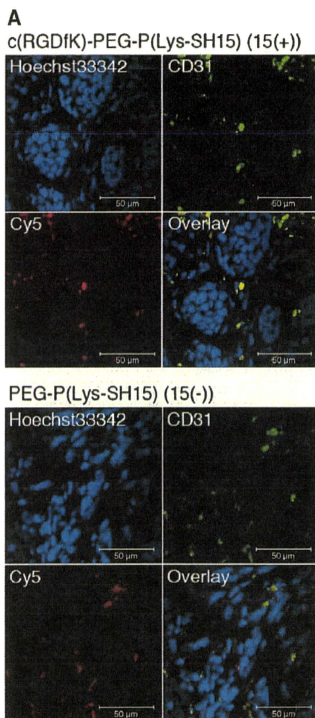


**Fig. 5.** In vivo tumor growth inhibition. RGD (+) and RGD (-) 15% crosslinked polyplex micelles loading plasmid DNA coding either sFlt-1 or Luc were administered intravenously to BxPC3 tumor bearing mice at a pDNA dose of 20  $\mu$ g on days 0, 4 and 8, as indicated by arrows. Control animals were injected with either Hepes buffer or 15 (+) micelle loading Luc expressing pDNA. Tumor volumes were measured every 2 days up to day 18 and normalized to the initial tumor volume (day 0). Results are presented in terms of relative tumor volumes, mean  $\pm$  s.d.,  $N = 6$ . \* $P < 0.05$  compared to control group.

pDNA was delivered in RGD(+) and RGD(-) crosslinked micelles. The most pronounced effect on microvessel density was observed with the plasmid administered in RGD(+) micelles. This is probably due to the combined effect of tumor accumulation and increased transfection efficiency of the RGD-conjugated 15% crosslinked polyplex micelle.

## 5. Conclusion

Our data contributes to the list of successful non-viral systems for antiangiogenic cancer gene therapy utilizing sFlt-1 pDNA as VEGF sequester [21,35] and RGD targeting of tumor endothelial cells [19,21]. Worth noting, the antiangiogenic gene therapy by sFlt-1 pDNA, delivered by non-viral vector with cRGD ligand, appears to be a promising strategy to treat an intractable pancreatic tumor.

The significant inhibitory effect of tumor growth shown in this study, confirms the potential of c(RGDfK)-PEG-P(Lys-SH15) and PEG-P(Lys-SH15) polyplex micelles as effective systemic gene delivery systems to the neo-vasculature of solid tumors. Both of these formulations showed accumulation and interaction with tumor endothelial cells. The therapeutic activity of c(RGDfK)-PEG-P(Lys-SH15) was pronounced by combined effect of increased tumor accumulation and enhanced intracellular delivery. Based on these studies, c(RGDfK)-PEG-P(Lys-SH15) can be employed as an effective platform for systemic administration of therapeutic plasmid DNA for antiangiogenic therapy.

## Acknowledgement

This work was financially supported in part by the Core Research Program for Evolutional Science and Technology (CREST) from Japan

**Fig. 4.** Micelle localization in tumor tissue. (A) Tumor endothelium and pDNA localization. Immunostaining of CD31 (green) revealed colocalization of Cy5-labeled pDNA (red) with tumor vasculature for both RGD-conjugated (15(+)) and non-conjugated (15(-)) micelles, 24 h after administration. The cell nuclei were stained with Hoechst 33342 (blue). (B) Quantitative analysis of Cy5-labeled pDNA (red pixels). The results represent percentage areas of pDNA-positive pixels per image. Seven images were taken from each tumor tissue, from 3 mice, mean  $\pm$  s.d.